CAMBRIDGE
UNIVERSITY PRESS

Mineral chemistry and thermobarometry of Jurassic arc granitoids: implications for petrotectonic and unroofing history of the southern Colombian Andes

Astrid Siachoque[1] , Daniel Alejandro García-Chinchilla[2], Sebastian Zapata[3], Agustín Cardona[1], Silvio Roberto Farias Vlach[2], Camilo Bustamante[4] and Luisa Fernanda Chavarría[5]

[1]Grupo de Estudios en Geología y Geofísica (EGEO), Departamento de Procesos y Energía, Facultad de Minas, Universidad Nacional de Colombia, Medellín, Colombia; [2]Department of Mineralogy and Geotectonics, University of Sao Paulo, Sao Paulo, Brazil; [3]Faculty of Natural Sciences, Universidad del Rosario, Bogota, Colombia; [4]Escuela de Ciencias Aplicadas e Ingeniería, Universidad EAFIT, Medellín, Colombia and [5]Department of Earth and Environmental Sciences, Michigan State University, East Lansing, MI, USA

Abstract

The Jurassic magmatic record in the southern Colombian (Northern Andes) includes numerous subduction-related I-type calc-alkaline granitoids with diverse structures and textures, formed in two main episodes at ~195 to 165 Ma and ~165 to 145 Ma. We provide new insights into the mineral chemistry, estimates of intensive parameters and petrogenetic processes of 12 plutonic occurrences in the region, grouped in 4 petrographic associations. Primary mineral assemblages include labradorite-to-oligoclase, alkali feldspars, ferroan enstatite, Mg-rich augite to ferroan-diopside, tschermakite to hastingsite and hornblende and Mg-rich annite; Fe-rich phlogopite and actinolite are post-magmatic phases. Amphibole chemistry indicates that the older (195–165 Ma) Jurassic bodies formed from relatively highly oxidized (f_{O_2} values buffered at $-0.1 \leq NNO \leq +1.4$) hydrous (~4 to 6 wt % H_2O) magmas and their differentiation involves significant crustal assimilation and/or magma mixing, fractional crystallization and late-magmatic re-equilibration processes. In contrast, the younger (165–145 Ma) Jurassic intrusives, derived from subducted-modified mantle sources, record moderately lower oxidized hydrous conditions (f_{O_2} values -0.7 to $0.8 \leq NNO$; ~5 wt % H_2O) with magma evolution mainly controlled by fractional crystallization and late-magmatic re-equilibration processes. Clinopyroxene-only, amphibole-only and amphibole-plagioclase thermobarometry estimations suggest that the Jurassic occurrences crystallized over variable temperature (647°C–1087°C) and pressure (0.7–6.3 kbar) conditions, corresponding to emplacement depths ranging from ~15, ~8 to 11, ~5 to 7 and <4 km along the arc crustal column. The obtained data combined with time evolution allow the identification of exhumed and fragmented arc blocks in the Jurassic magmatic system and provide an essential link between the orogenic deformation event poorly constrained in the Northern Andes.

1. Introduction

Jurassic magmatism in the Northern Andes is widely exposed in the central and eastern segments of the Colombian Cordilleras, representing the vestiges of the subduction history of the Farallon Plate under the South American continent, after the amalgamation and the beginning of the break-up of the Pangea supercontinent (Bustamante *et al.* 2010; Cochrane *et al.* 2014a; Spikings *et al.* 2015; Bustamante *et al.* 2016; Zapata *et al.* 2016; Quandt *et al.* 2018; Rodríguez *et al.* 2018; García-Chinchilla and Vlach, 2019; Leal-Mejía *et al.* 2019; Rodríguez-García *et al.* 2020a; Restrepo *et al.* 2021; Rodríguez-García *et al.* 2022). The spatial-temporal and compositional characteristics of the Jurassic plutonic rocks in southeastern Colombia reveal a protracted arc-related magmatic history spanning ~60 Ma. This magmatic activity initiated around 195 Ma and continued into the early Cretaceous (~130 Ma), with distinct tectono-magmatic processes occurring during two main intervals. The older phase, which persisted until ~165 Ma, is marked by predominantly calc-alkaline high-K granitoids. The spatial distribution of these granitoids has been attributed to either an eastern cratonward migration of the arc coupled with subduction erosion (Rodríguez *et al.* 2018) or as part of a long-term stationary arc where magmatic fluxes varied over time (Bustamante *et al.* 2019). Plutonic bodies associated with the youngest interval (~165 to 145 Ma) are also calc-alkaline medium-K arc-related. Some of them exhibit particularly complex deformational relations and are contemporaneous with a

regional metamorphic event (Blanco-Quintero *et al.* 2014; Bustamante *et al.* 2016; Quandt *et al.* 2018; Rodríguez-García *et al.* 2020a; Restrepo *et al.* 2021).

Despite the major advances in the reconstruction of this tectono-magmatic evolution and the paleogeographic configuration of the Northern Andes between the Jurassic and the Early Cretaceous (Bayona *et al.* 2020), there are still unresolved aspects that need further investigation. These include the rigorous testing of different hypotheses regarding the petrological processes involved in the formation of arc magmas, i.e. magma sources, the role of fractional crystallization, recharge, crustal assimilation or magma mixing/mingling processes, that can be used as a first-order input for the regional tectonic models. Additionally, the influence of exhumation events on the current crustal architecture, particularly the structural levels exposed by various plutonic and volcanic units that constitute different remnants of the arc, and their relationship with the Andean history, needs to be thoroughly examined.

Mineral chemistry of magmatic phases in igneous rocks offers valuable tools to investigate crystallization conditions and magmatic processes. The compositions of feldspars, pyroxene, amphibole, biotite and Fe–Ti oxides minerals have been widely used to estimate key intensive parameters such as crystallization pressure and temperature of intrusive rocks in arc magmatic systems (Kazemi *et al.* 2018; Bastos *et al.* 2021; Cui *et al.* 2021; Lima *et al.* 2021; Molina *et al.* 2021; Schaaf *et al.* 2021; Zandomeni *et al.* 2021; Yan *et al.* 2022; Zaheri-Abdehvand *et al.* 2022). In detail, compositions of magmatic amphibole serve as another proxy to determine the redox conditions and water contents of the parental magmas in arc-related rocks (Ridolfi *et al.* 2010; Ridolfi and Renzulli, 2012; Erdmann *et al.* 2014; Ridolfi, 2021).

This contribution focuses on the examination of textural and chemical features of rock-forming mineral phases such as feldspar, pyroxene, amphibole and biotite group-minerals of selected samples from 12 calc-alkaline I-type occurrences exposed in the southern region of Colombia with ages between ~195 to 165 and ~165 to 145 Ma, to discuss crystallization conditions and emplacement depths. This will allow us to understand the different magmatic processes that formed these granitoids and specially evaluate the processes that may have caused the differences between the two major magmatic intervals. Due to the local discordant relations of these intrusive bodies and their associated volcanic rocks with Early Cretaceous clastic sediments, we will explore the nature and significance of Late Jurassic to Early Cretaceous exhumation event and its relationship with the complex re-organization experienced by the margin during this time interval (Bayona *et al.* 2020).

2. Geological setting

The Northern Andes has been an active convergent margin since the Paleozoic, recording a prolonged subduction at the western margin of Gondwana. This region has been characterized by the development of continental magmatic arcs, marked by the emplacement of extensive volumes of igneous rocks (Bustamante *et al.* 2016; Leal-Mejía *et al.* 2019; Rodriguez-Garcia *et al.* 2019; Spikings and Paul, 2019; Bayona *et al.* 2020; Rodríguez-García *et al.* 2020b; Restrepo *et al.* 2023). As a result, the geological and structural configurations of the Colombian Andes, which encompass the Western, Central and Eastern Cordilleras (WC, CC and EC; Fig. 1a), have been shaped by this subduction zone.

The long-term subduction of the Farallon plate beneath the western margin of South America, inferred from whole-rock geochemical and geochronological data is associated with extensive arc-like magmatism during late Triassic to early Cretaceous (Bustamante *et al.* 2010; Cochrane *et al.* 2014a; Bustamante *et al.* 2016; Zapata *et al.* 2016; Quandt *et al.* 2018; Rodríguez *et al.* 2018; Leal-Mejía *et al.* 2019; Ramírez *et al.* 2020; Rodríguez-García *et al.* 2022). This period witnessed the emplacement of I- and minor S-type intrusions together with mafic, intermediate and acid volcanic and subvolcanic rocks. Overall, they are calc-alkaline rocks with metaluminous signatures, suggesting a continental volcanic arc affinity (Rodríguez-García *et al.* 2020a).

Chavarria *et al.* (2021) suggest that the initial phase of Early Jurassic arc magmatism involved crustal thickening due to the underplating of high volumes of magmas until ~165 Ma. Then, the subduction in the Middle Jurassic was marked by a more oblique convergence between the northwestern margin of Gondwana and the Farallon plate, resulting in a reduction of the magma volumes (Bustamante *et al.* 2016). An additional Late Jurassic tectonic event (*c.* 158 Ma) involved the formation of a collision-related metamorphic belt, which has been identified in faulted contact with the arc-related batholiths (Blanco-Quintero *et al.* 2014; Bustamante *et al.* 2017, 2023; Restrepo *et al.* 2021). This regional metamorphism may have occurred due to the oblique collision of a para-autochthonous terrane during the evolution of the northwestern margin of Gondwana (Blanco-Quintero *et al.* 2014), also causing the deformation of some of the Jurassic plutonic occurrences in the region (e.g. Sombrerillo and Ibague Batholiths; Restrepo *et al.* 2021; Bustamante *et al.* 2023). After this collision, the margin may have experienced a crustal thinning event, leading to a progressive decrease in the magmatic activity until Early Cretaceous Period (~129 Ma) (Bustamante *et al.* 2016; Chavarría *et al.* 2021).

The long-lived Mesozoic magmatic record can be also separated in two main regions comprising the southern plutons between ~1 and 5° N and those exposed in the northern part between ~6 and 12° N of latitude (Fig. 1b). For this study, we focus on the widely exposed calc-alkaline I-type bodies in the southern region of Colombia (Fig. 1c), which were emplaced between ~195 to 165 and ~165 to 140 Ma in the Upper Magdalena Valley (UMV) and the Southern Central Cordillera (SCC) domains, respectively.

The UMV domain is a hinterland basin located between the CC and the EC of Colombia formed during the Miocene (e.g. Espitia *et al.* 2022; Ramon and Rosero, 2006; Saeid *et al.* 2017; Villamizar-Escalante *et al.* 2021). This tectonic domain includes diverse crustal lithologies varying from Meso- and Neoproterozoic high-grade metamorphic basement rocks (Ibañez-Mejia, 2020); Paleozoic sedimentary units (Villamizar-Escalante *et al.* (2021); Permian high-grade metamorphic and plutonic rocks (Restrepo *et al.* 2023; Rodriguez-Garcia *et al.* 2019; Rodríguez *et al.* 2017); and Triassic sedimentary formations. These basement rocks were intruded by intermediate to felsic Jurassic plutons formed from ~195 to 169 Ma (Rodríguez *et al.* 2018) and covered by contemporaneous and associated volcanic and volcano-sedimentary sequences (Rodríguez-García, 2018). Aptian-Albian sedimentary units overlap Jurassic intrusive rocks. These Cretaceous unconformities were observed overlaying several of the basement blocks containing the Jurassic plutonic units (Fig. 1c).

The SCC domain is mostly composed of Permian and Triassic low- to high-grade metamorphic and plutonic basement rocks (Bustamante *et al.* 2017, 2023; Rodriguez-Garcia *et al.* 2019). This
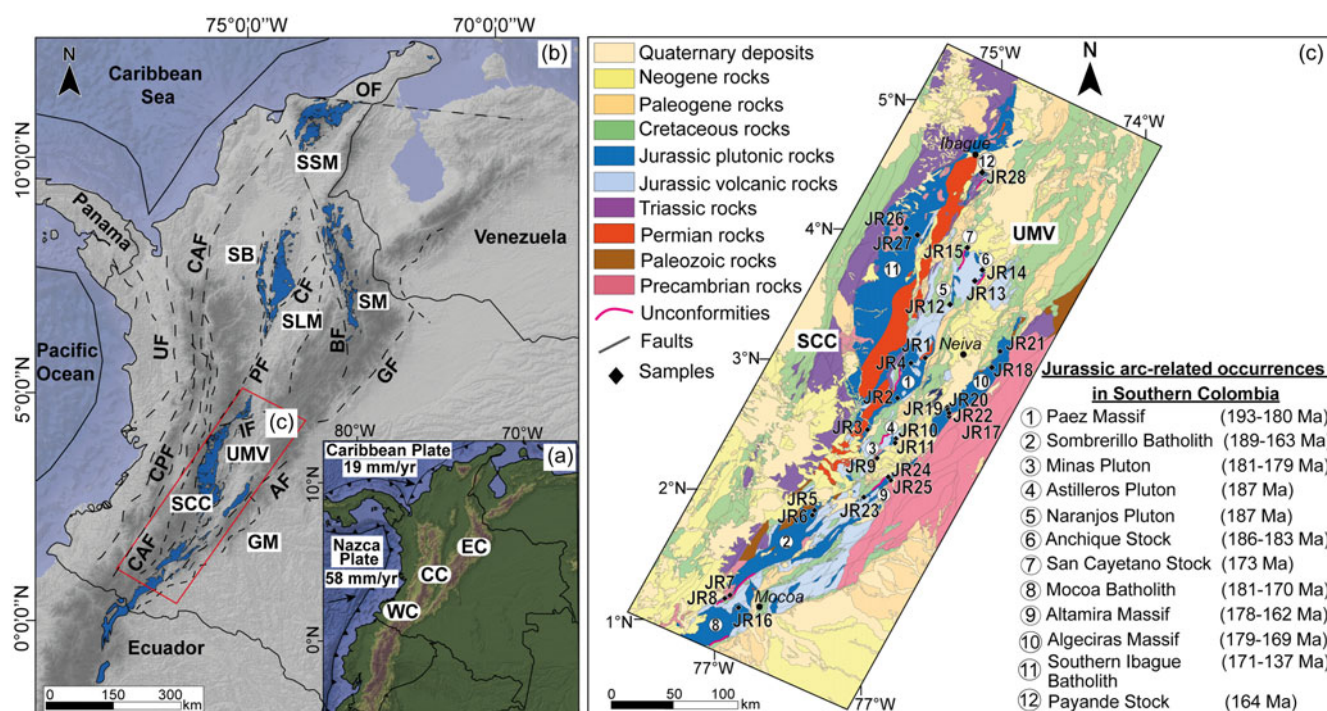
Figure 1. (Colour online) Geological setting of the Northern Andes and location of the study area. (a) The main topographic features of the region highlight the Western (WC), Central (CC), and Eastern (EC) Cordilleras of Colombia. (b) Distribution of the late Triassic to Early Cretaceous plutonic belt in the Colombian Andes with the main tectono-magmatic domains and faults systems (adapted from García-Delgado *et al.*, 2022). Abbreviations: SM, Santander Massif; SMM, Santa Marta Massif; SB, Segovia Batholith; SLB, San Lucas Batholith; UMV, Upper Magdalena Valley; SSC, Southern Central Cordillera; GM: Garzon Massif; OF, Otu Fault; CPF, Cali-Patia Fault; UF, Uramita Fault; CAF, Cauca-Almaguer Fault; CF, Cimitarra Fault; PF, Palestina Fault; IB, Ibague Fault; GF, Guaicaramo Fault; BF, Bucaramanga Fault; AF, Algeciras Fault. (c) Geological map of the Southern Colombian Andes (adapted from Gomez *et al.*, 2019). The map indicates the collected samples from the studied Jurassic arc-related plutonic occurrences.

basement is intruded by the Jurassic-early Cretaceous Ibague batholith and locally by the Payande stock, both characterized by mafic to intermediate compositions (Bustamante *et al.* 2010; Cochrane *et al.* 2014b; Bustamante *et al.* 2016; Leal-Mejía *et al.* 2019; Rodríguez-García *et al.* 2020a, 2022). The batholith is divided into the southern (~171 to 150 Ma) and northern (~152–137 Ma) segments (Rodríguez-García *et al.* 2020a, 2022), in which the latter has been spatial-temporally related to a regional metamorphic event forming late Jurassic units with low- to medium-grade metamorphic rocks (Blanco-Quintero *et al.* 2014; Bustamante *et al.* 2017; Zapata-García *et al.* 2017; Bustamante and Bustamante, 2019; Restrepo *et al.* 2021). Field and petrography evidence suggest the development of magmatic to submagmatic foliation and solid-state mylonitic deformational fabrics within the northern segment of this batholith (Rodríguez-García *et al.* 2020a, 2022).

Well-defined angular discordances between Triassic and Jurassic sediments and volcanic rocks of the Jurassic plutons and Early Cretaceous (Albian-Aptian) sediments have been also documented in these regions (Bayona *et al.* 2020). Despite these unconformities imply the exhumation of the Jurassic volcanic arc, the limited sedimentary record and the thermal resetting of low-temperature thermochronological systems during the Early Cretaceous have hindered the reconstruction of the Late Jurassic to Early Cretaceous exhumation and deformation histories of the NW South America continental margin (~160 to 120 Ma). Since the middle to Late Cretaceous, the onset of the Andean orogenic phases promoted the uplift and exhumation of basement units in the Central Cordillera and the UMV, causing a vertical re-organization of the Jurassic magmatic arc (Ramon and Rosero,

2006; Montes *et al.* 2019; Villamizar-Escalante *et al.* 2021; Zapata *et al.* 2023).

3. Sampling, methods and data analysis

We studied 12 different Jurassic intrusive bodies along the UMV and SCC domains shown in Fig 1c, including the (1) Paez Massif, (2) Sombrerillo Batholith, (3) Minas Pluton, (4) Astilleros Pluton, (5) Naranjos Pluton, (6) Anchique stock, (7) San Cayetano Stock, (8) Mocoa Batholith, (9) Algeciras Massif and (10) Altamira Massif within the UMV domain, and the (11) Southern Ibague Batholith and (12) Payande Stock located within the SCC domain. These intrusive bodies are bounded by regional fault systems, namely: the Algeciras Fault, Agrado-Betania Fault, La Plata-Chusma Fault, Frailes-Pava Fault and Ibague Fault (Fig. 2). Essential geochemical and geochronological (U-Pb in zircon ages) data from the studied plutonic occurrences are summarized in Table 1.

Sampling for this study was conducted on representative localities (see locations in Fig 1c). The selection of sample sites considered previous petrographic, geochronological and geochemical information (Table 1). The complete dataset comprises 25 samples obtained from 10 occurrences located in the eastern-most UMV domain. In this region, the plutonic rocks intrude Precambrian basement rocks and are spatially related to Jurassic volcanic sequences (Fig. 1c). Additionally, three samples were collected from two occurrences in the SCC domain, which are exposed in the westernmost part of the study area, where they intruded Triassic to Permian metamorphic and plutonic basement rocks, respectively (Fig. 1c). Collected plutonic samples were then subjected to broad petrography and mineral chemistry analysis.
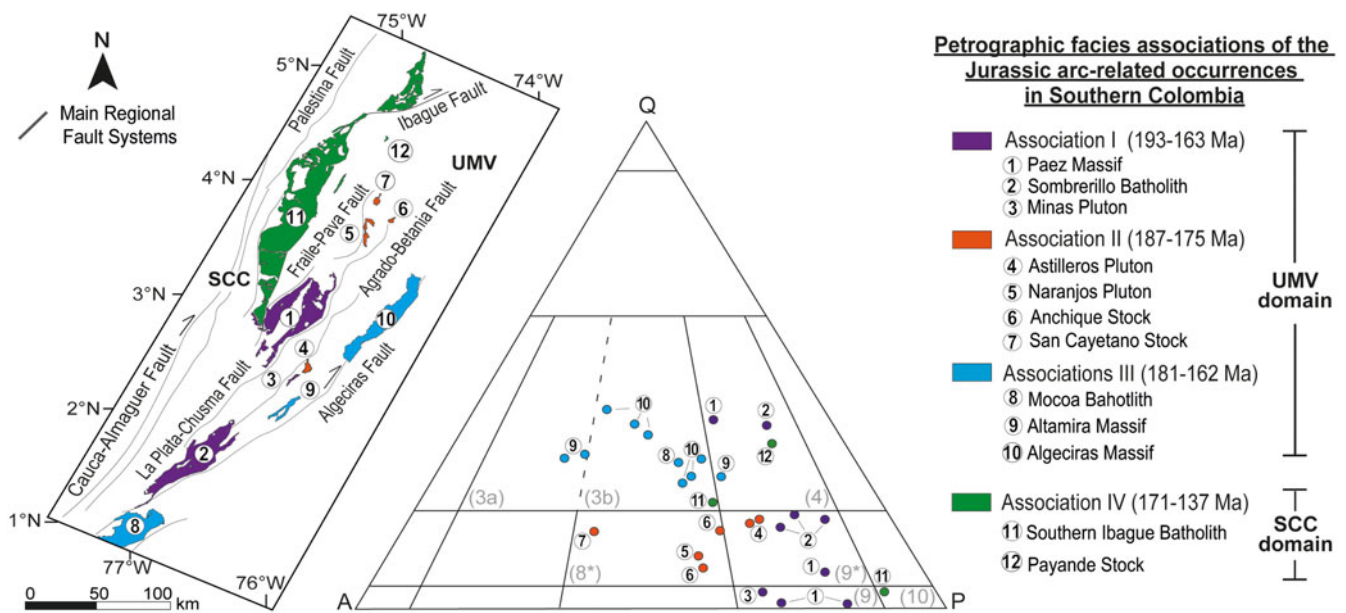
Figure 2. (Colour online) Modal classification of the studied samples in the QAP modal classification diagram (Le Maitre *et al.*, 2002; Streckeisen, 1976) and the distinction of the four main petrographic facies associations proposed for the Jurassic arc-related occurrences in Southern Colombia. Numbered fields: (3a) syenogranite; (3b) monzogranite; (4) granodiorite; (8*) quartz monzonite; (9*) quartz monzodiorite; (9) monzodiorite; (10) gabbro/diorite.

3.a. Petrographic associations

A petrographic facies refers to a descriptive unit, which can be recognized and described in hand samples and in field outcrops through its structural, textural and mineralogical features. Conversely, a petrographic-facies association represents a mapping unit for a given map scale and may group one or more petrographic facies (Ulbrich *et al.* 2001).

Among the studied intrusive occurrences, the Altamira and Algeciras Massifs in the Eastern Cordillera of Colombia are the unique occurrences mapped in some detail (García-Chinchilla and Vlach, 2019), using the concepts of petrographic-facies and facies associations. The other intrusive bodies, in spite of the available petrographic, geochemical and geochronological information, have not been mapped in any detail and thus the constituting petrographic facies (e.g. dioritic, tonalitic, granodioritic and granitic varieties), their relative proportions and structural relations, as well as the main constituting intrusive units or plutons are not properly known.

Considering these limitations and the available information, we chose to group the studied occurrences according to some general petrographic associations, defined mainly by their geographic distribution, petrographic, compositional and age variation ranges. In these senses, these petrographic associations are descriptive geological units which may arguably correspond to the units and super-units as defined in the Coastal Batholith of Peru (e.g. Cobbing and Pitcher, 1983), as more basic geological data are acquired. This approach allowed us to define four main petrographic-facies associations I, II, III and IV, within the studied Jurassic occurrences in southern Colombia; among them, three crops out in the UMV domain and the other in the SCC domain.

3.b. Petrography and mineral chemistry

Petrography analyses focused on mineralogical and textural properties to define petrographic facies and magma series (see the following section). All samples were examined in polished thin (30 μm in thick) sections under a petrographic microscope, using transmitted and reflected lights. Quantitative modal data were obtained with a chariot and a manual point counter and are depicted in Fig. 2 and presented in Supplementary Table S1. After the petrography work, the thin-sections were carbon coated for electron microprobe (Electron Probe Micro-Analyzer - EPMA) analysis, which included electron-backscattering imaging and spot analysis by qualitative energy-dispersive spectrometry and quantitative wavelength-disperse spectrometry (WDS).

The EPMA work was done in two separate analytical phases. Twenty-four samples were analyzed using a field emission JEOL JXA-FE-8530 microprobe at the laboratories of the GeoAnalitica core facility, Institute of Geosciences of the University of São Paulo, Brazil. WDS analysis was performed with 15 kV, 20 nA and 5 μm for the column acceleration voltage, beam current and beam diameter, respectively. Total counting times, equally distributed for peak and background readings, varied from 10 s (major and light elements) to 40 s (minor elements); matrix effects were corrected with the *PROZA* PRZ/Armstrong software. We used natural and synthetic standards from both the Smithsonian and the GellerTM collections: hornblende (Si and Al in amphiboles), diopside (Mg), fayalite (Fe and Mn), anorthoclase (Al), wollastonite (Ca), orthoclase (K), rutile (Ti), albite (Na), zircon (Zr), willemite (Zn), benitoite (Ba), glass_synthetic (Ni) sodalite (Cl) and fluorapatite (F). Other four samples were analyzed with a conventional JEOL JXA-8230 microprobe at the Department of Petrology and Metalogenesis, Institute of Geosciences of the University of Rio Claro, Brazil, under the same analytical conditions, except for the counting times settled at 10 s and 20 s for major and minor elements, respectively, and the standards used for element calibrations, which were wollastonite (Ca), orthoclase (Si and K), albite (Na), diopside (Mg), anorthite (Al), ilmenite (Ti and Fe), chromite (Cr), rhodonite (Mn), synthetic NiO (Ni), sodalite (Cl) and barite (Ba). Of note, Al was repeaked over hornblende from the samples to avoid Al peak shift in this latter case.

Mineral formulae for the analyzed pyroxene, feldspar, biotite and amphibole-group minerals were determined based on 6, 8, 11

Table 1. Compilation of the geochemical and geochronological (U-Pb in zircon ages) data of the studied Jurassic arc-related occurrences

Tectonic domain	Occurrence	Area km²	Lithology	Age (Ma)	Mean major and trace element compositions										La/ Yb	Sr/ Y	Temperatures	
					SiO_2	Ti_2O	Al_2O_3	MgO	CaO	K_2O	Mg#	ASI	LILEs	REEs			$Tsat_{Ap}$	$Tsat_{Zr}$
UMV	Paez Massif	~1300	Monzodiorites and Qz monzodiorites	189–181	56.9	0.9	16.4	4.3	7.3	2.0	42.8	0.79	1265	114	10	27	891°	–
			Granodiorites	180	68.0	0.5	15.3	2.0	3.1	2.4	40.7	1.03	1177	90	15	45	882°	736°
	Sombrerillo Batholith	~1245	Qz monzodiorites	189–181	58.4	0.9	17.0	3.1	6.0	3.3	45.9	0.86	1861	162	13	14	910°	–
			Granodiorites	173–163	65.4	0.6	14.5	1.2	3.1	3.4	35.3	0.88	1660	150	16	16	898°	–
	Minas Pluton	~9	Qz monzodiorites	181	58.1	0.9	17.2	3.0	6.0	2.2	44.5	0.89	1445	139	10	29	892°	–
	Astilleros Pluton	~20	Qz monzodiorites	187	63.3	0.8	15.9	2.2	4.3	3.3	32.5	0.92	1428	163	10	13	897°	–
	Naranjos Pluton	~47	Qz monzonites	187	65.1	0.7	15.6	2.1	3.9	4.5	30.4	0.87	1845	241	14	13	909°	–
	Anchique Stock	~8.5	Qz monzonites	183	64.6	0.7	15.0	2.2	3.4	4.3	36.2	0.91	2186	252	24	26	926°	–
	San Cayetano Stock	~21	Qz monzonites	173	58.3	0.8	17.2	2.5	5.1	3.5	31.3	0.92	1568	202	12	18	875°	–
	Mocoa Batholith	~1675	Granites	181	70.1	0.4	14.6	0.8	2.0	4.9	30.4	1.01	2056	176	18	17	893°	718°
	Algeciras Massif	~110	Granites	176–168	71.3	0.3	14.1	0.9	1.8	4.5	34.2	0.96	1261	192	24	14	933°	738°
	Altamira Massif	~455	Granodiorites and Granites	179–162	66.2	0.3	17.5	0.4	2.0	5.3	23.6	0.97	1570	265	27	15	894°	753°
SCC	Southern Ibague Batholith	~3200	Diorites and Tonalites	171–159	60.0	0.8	17.0	3.3	6.7	1.8	52.3	0.90	834	105	8	13	906°	–
			Granodiorites and Granites	157–137	66.8	0.6	15.4	1.7	4.1	2.5	44.4	1.03	1197	119	13	17	877°	706°
	Payande Stock	~7	Granodiorite	164	67.7	0.4	15.2	2.1	3.7	3.9	53.4	1.03	1083	59	–	28	881°	678°

Mg#: molar(100×MgO/(MgO+FeO$_T$)); ASI: molar Al$_2$O$_3$/(Na$_2$O+K$_2$O+CaO); LILEs and REEs in ppm. Data from Bustamante *et al.* (2010, 2016); Chavarría *et al.* (2021); Leal-Mejía *et al.* (2019); Restrepo *et al.* (2021); Rodríguez *et al.* (2018); Rodríguez-García *et al.* (2020b, 2022).

and 24 atoms per formulae unit (apfu), respectively. The classifications of pyroxenes, feldspars and biotite follow Rock (1990), Deer *et al.* (2013) and Tischendorf *et al.* (2007), respectively. In the case of biotite mineral formulae, Tischendorf's formula [$Li_2O = 2.1/(0.356 + MgO) − 0.088$] has been used to estimate the Li contents (Tischendorf *et al.* 2004). The amphibole-group classification was considered according to the scheme of Hawthorne *et al.* (2012), by using the Excel spreadsheet of Locock (2014). The compositional results for all minerals and their calculated structural formulae are given in Supplementary Tables S2b to S2d.

Thermobarometry calculations were applied to selected minerals in most of the studied rocks using the Online MagMin_PT Geothermobarometry Program for magmatic rocks developed by Gündüz and Asan (2022). Compositions of clinopyroxene were useful to calculate magma pressures and temperatures according to the thermobarometer of Wang *et al.* (2021). We selected plagioclase–hornblende pairs for temperature estimations using the thermometry model of Holland and Blundy (1994) (expression B) and for pressure estimations, we applied the barometric expression of Molina *et al.* (2015). These pairs were based on the compositions of plagioclase and amphibole crystal rims in contact, where the two phases are most likely to have been in textural exchange reaching magmatic equilibrium conditions (Blundy and Cashman, 2008). Amphibole compositions from crystal rims were also used to compare the above P-T estimations with those of the Al-in-hornblende barometer of Mutch *et al.* (2016) and Ti-Amp thermometer of Liao *et al.* (2021) as well as to constraint some physicochemical crystallization conditions such as log f_{O_2} and H_2O-in-melt, applying the chemometric empirical expressions of Ridolfi (2021).

4. Results

Based on the available geologic information and the newly obtained petrography and mineralogical data, we defined four distinct Jurassic petrographic associations in southern Colombia, as described in the following section. The UMV domain includes three of these associations (I, II and III) with emplacement ages spanning from ~193 to 162 Ma. In contrast, the fourth association (IV), situated in the SCC domain, presents somewhat younger ages ranging from ~171 to 137 Ma (Fig. 2).

4.a. Petrography

The modal classification of the studied samples is illustrated in Fig. 2, which provides a visual representation of the spatial-temporal variations and compositional features observed among the studied plutons.

The petrographic association I is made up of mesocratic and leucocratic dark-grey and greyish-coloured rocks, including massive to slightly foliated monzodiorites, quartz monzodiorites and granodiorites from the Paez Massif, Sombrerillo Batholith and Minas Pluton in the western part of the UMV domain (Fig. 2). These rocks are primarily intrusive into Precambrian basement rocks and record the older magmatic activity, between *c.* 193 and 163 Ma. The petrographic association II includes mesocratic to leucocratic grey- and pinkish-coloured quartz monzodiorites and quartz monzonites from the San Cayetano and Anchique stocks, and the Naranjos and Astilleros plutons exposed in the central part of the UMV domain (Fig. 2). The plutons characterized by this facies group were emplaced from ~185 to 175 Ma and intrude

relatively contemporaneous Jurassic volcanic rocks of the Saldaña Formation to whom they are probably related (Fig. 1c). The petrographic association III comprises leucocratic grey- and pinked-coloured granodiorites and granites from the Mocoa Batholith, and the Algeciras and Altamira massifs, cropping out in the eastern part of the UMV domain (Fig. 2). They record emplacement ages ranging from 181 to 162 Ma, intrude Precambrian rocks and are also closely associated with the volcanic rocks of the Saldaña Formation (Fig. 1c). The last association IV presents the most expanded compositional variation, including mesocratic and leucocratic dark-green- and grey-coloured diorites, granodiorites and monzogranites, respectively, from the southern Ibague Batholith and the Payande Stock located in the SCC domain (Fig. 2). These occurrences represent the latest magmatic record in the study area (*c.* 171–137 Ma) and intrude mainly Triassic to Permian basement rocks. The main petrographic characteristics of these associations are summarized in Supplementary Table S2. Some additional petrographic features are provided below.

4.a.1. Association I
This association include medium-to-coarse-grained and equi-to-inequigranular textures (Table S2). The quartz monzodiorite and monzodiorite facies exhibit well-developed corona textures, where euhedral to subhedral orthopyroxene and/or clinopyroxene crystals are rimmed and partially replaced by amphibole or biotite (Fig. 3a,b). Of note, orthopyroxene was exclusively found in quartz monzodiorites from the Sombrerillo Batholith, which are the unique two-pyroxene-bearing rocks known in the whole studied area. Some clinopyroxene crystals display exsolution lamellae of pigeonite and sieved cores and occasionally occur in intergrowths with plagioclase. Plagioclase is euhedral to subhedral and has tabular habits. It exhibits concentric or discontinuous oscillatory zoning patterns (Fig. 4a), especially in the granodiorite facies, where crystals show strong saussurite alteration (Fig. 3c). Amphibole is the most abundant mafic phase in all facies occurring either as isolated crystals or forming mafic aggregates with biotite, Fe–Ti oxides and titanite. They usually form euhedral to subhedral crystals with prismatic habits and brownish-green pleochroism (Fig. 3c). Biotite is commonly found in association with amphibole, displaying textures suggestive of co-precipitation (Fig. 3a). It forms subhedral platy crystals of fine to medium grain size, showing brownish-green pleochroism and containing small inclusions of euhedral apatite and zircon. Biotite often undergoes chlorite alteration. K-feldspar is late magmatic and anhedral. In the monzodiorite and quartz monzodiorite facies, it occurs interstitial to plagioclase and amphibole euhedral crystals, resembling some extent cumulate textures (Fig. 3c and Fig. 4b), whereas, in the granodioritic facies, it usually forms subhedral coarse-grained crystals, partially sericitized and closely related with quartz. The accessory minerals in this group are mainly magnetite, titanite, apatite and zircon. Chlorite, epidote, carbonates, sericite/muscovite and albite are post-magmatic substituting the primary phases.

4.a.2. Association II
This association present a predominant massive structure and fine- to medium-grained inequigranular, porphyritic textures (Table S2). Clinopyroxene occurs as grouped subhedral crystals closely related to Fe–Ti oxides, amphibole and biotite. Many of the crystals also exhibit exsolution lamellae and are partially replaced either by biotite or chlorite along cleavage planes (Fig. 3d). Clinopyroxene rimmed by chlorite is also found (Fig. 4c).
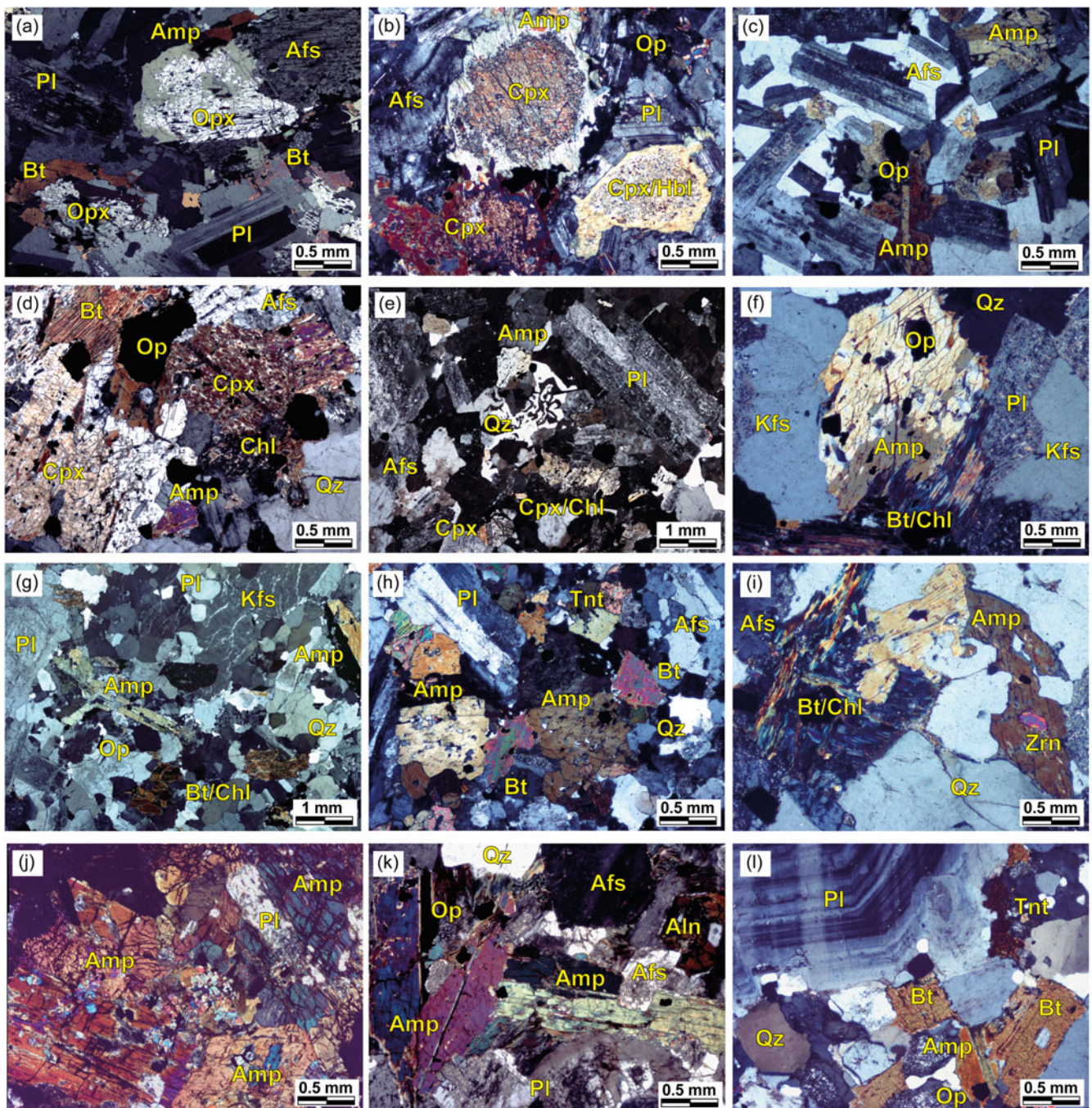
Figure 3. (Colour online) Microtextural features of rock-forming minerals from the Jurassic arc-related plutonic occurrences in southern Colombia. Photomicrographs under crossed polarized light: (a) Orthopyroxene crystals in reaction texture within hornblende and biotite. (Association I - Sample JR5); (b) Corona of hornblende around clinopyroxenes (Association I - Sample JR1); (c) Euhedral plagioclase crystals and aggregates of amphibole and opaques minerals enclosed by interstitial K-feldspar (Association I – Sample JR3); (d) Clinopyroxene grouped crystals with inclusions of apatite and in close relation with biotite and opaque minerals (Association II - Sample JR14); (e) Graphic quartz-orthoclase intergrowth and isolated clinopyroxenes crystals partially replaced by chlorite (Association II - Sample JR15); (f) Prismatic amphibole with inclusions of opaques and in reaction with pseudomorphic chlorite crystals after biotite (Association II - Sample JR13); (g) Inequigranular texture with concentric zoning plagioclase and perthitic alkali feldspar phenocrysts and isolated amphibole and biotite crystals (Association III - Sample JR17); (h) Mafic aggregate of amphibole, biotite, titanite and opaques crystals (Association III - Sample JR25); (i) Amphibole with inclusions of opaques and zircon and in co-precipitation texture with pseudomorphic chlorite after biotite (Association III – Sample JR16); (j) Coarse-grained hornblende and plagioclase grouped crystals forming cumulate-like texture (Association IV - Sample JR26); (k) Amphibole grouped crystals showing prismatic and elongated habits and in close relation to primary plagioclase (Association IV - Sample JR27); (l) Oscillatory zoning in plagioclase phenocryst in contact with primary biotite crystals (Association IV - Sample JR28). Mineral abbreviations according to Warr (2021).

Plagioclase occurs as large subhedral tabular crystals, showing microcracks, saussuritic cores and reabsorbed rims (Fig. 3e). Amphibole occurs in two textural types: the first consists of large prismatic individual crystals with slight greenish pleochroism,

sometimes showing poikilitic textures with abundant small magnetite and apatite inclusions. Some crystals occur in equilibrium texture with biotite (Fig. 3f), suggesting co-precipitation. The second type of amphibole is present as colourless fine
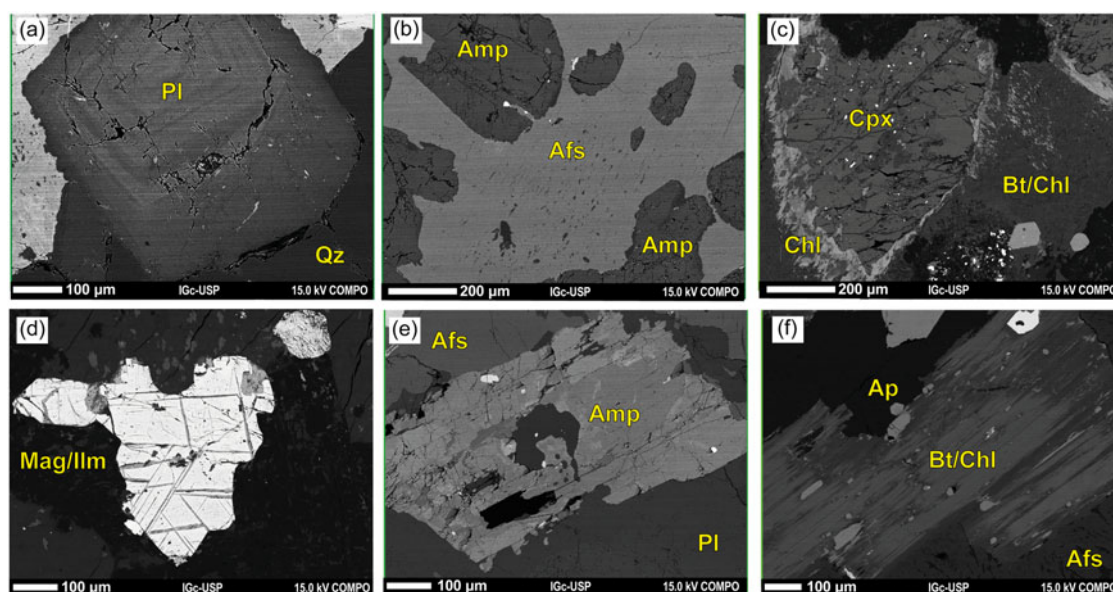
Figure 4. (Colour online) BSE images of rock-forming minerals from the Jurassic arc-related plutonic occurrences in southern Colombia. (a) Euhedral plagioclase showing oscillatory zoning pattern (Association III - Sample JR24); (b) Poikilitic groundmass K-feldspar including several hornblende crystals (Association I - Sample JR3); (c) Reaction rims of biotite-chlorite around clinopyroxene (Association II - Sample JR12); (d) Magnetite host crystals (light white) with thin trellis-type lamellae exsolution of ilmenite in dark grey (Association II - Sample JR14); (e) Subhedral hornblende crystals with patchy zoning pattern and microcracks (Association III - Sample JR17); (f) Euhedral biotite crystal partially replaced by chlorite represented by the main darker area (Association III - Sample JR25). Mineral abbreviations according to Warr (2021).

intergrowths within primary amphiboles or as acicular interstitial crystals between felsic minerals in the groundmass, suggesting a post-magmatic origin. Biotite also exhibits two textural types: one group consists of subhedral lamellar medium-grained greenish-brownish crystals, closely associated with the first generation of amphibole and partially altered to chlorite (Fig. 3f), while the other type is characterized by aggregates of fine-grained flakes intergrowing with chlorite or epidote and replacing clinopyroxene, indicating a likely post-magmatic, hydrothermal origin (Fig. 3d). Mymerkite intergrowths along perthitic K-feldspar and plagioclase boundaries and graphic intergrowths between K-feldspar and quartz are widespread in these rocks (Fig. 3e). Euhedral magnetite showing trellis-type lamellae of exsolved ilmenite (Fig. 4d) and titanite are the main accessories for these rocks, being accompanied by minor allanite, apatite and zircon. Samples from this group are also characterized by strong pervasive hydrothermal alteration leading to the precipitation of a significant amount of hydrothermal minerals, which besides those observed in Association I include common prehnite.

4.a.3. Association III

The rocks in this association exhibit massive structures with variable fine- to coarse-grained equi- to inequigranular textures (Table S2). Amphibole is the predominant mafic phase, occurring either as individual crystals or forming mafic clots along with biotite, Fe–Ti oxides and titanite (Fig. 3g). The crystals are euhedral to subhedral with prismatic habits and contain inclusions of zircon, Fe–Ti oxides and allanite (Fig. 3h). Some amphiboles display patchy and/or reabsorbed textures and related microcracks (Fig. 4e) and may show exsolution Fe–Ti oxides along cleavage planes. Plagioclase occurs as large euhedral to subhedral tabular crystals with oscillatory and concentric zoning patterns. In some cases, plagioclase crystals show highly altered cores and unaltered rims (Fig. 3g). Biotite is a late-crystallized mafic, forming interstitial subhedral to anhedral platy fine-grained crystals that

are commonly replaced by chlorite (Fig. 3i and 4f). K-feldspars form subhedral medium-grained perthitic crystals, occurring in close relation with quartz (Fig. 3h). Locally, mymerkite intergrowths are observed. The accessory phases are the same as described for the previous associations; however, some magnetite crystals are rimmed and partially substituted by titanite. The alteration minerals also include some hematite and pyrite.

4.a.4. Association IV

The rocks included in this association have massive structures and fine- to coarse-grained inequigranular textures (Table S2). Some rocks of the diorite facies present coarse euhedral plagioclase and amphibole aggregates, resembling cumulate-like textures (Fig. 3j). Amphibole is also the main mafic mineral, crystallizing as groups of relatively larger prismatic, euhedral to subhedral, twinned crystals with dark green to brown pleochroism (Fig. 3k). Some among them display poikilitic textures with a significant number of inclusions of Fe–Ti oxides, titanite, apatite and some allanite. Fe–Ti oxides (mainly ilmenite) are observed along their cleavage planes (Fig. 3j). Biotite occurs in two different types: one consists of large subhedral crystals with small mineral inclusions of apatite and zircon, showing yellow-brown pleochroism and placoid habits; the other forms aggregates of fine-grained flakes interstitial between the felsic minerals, associated with secondary chlorite, epidote and/ or carbonates (Fig. 3l). Plagioclase crystallizes as large well-formed tabular crystals with distinct concentric, oscillatory zoning textures and strongly saussuritic cores (Fig. 3l). K-feldspar is present as subhedral medium-grained twinned crystals closely associated with quartz and shows some albite lamellae exsolution. Pseudomorphic chlorite after biotite is observed in all samples from this petrographic association.

4.b. Mineral compositions

Our EPMA dataset includes chemical analyses of feldspar (518), pyroxenes (39), amphiboles (310) and biotite (182) group
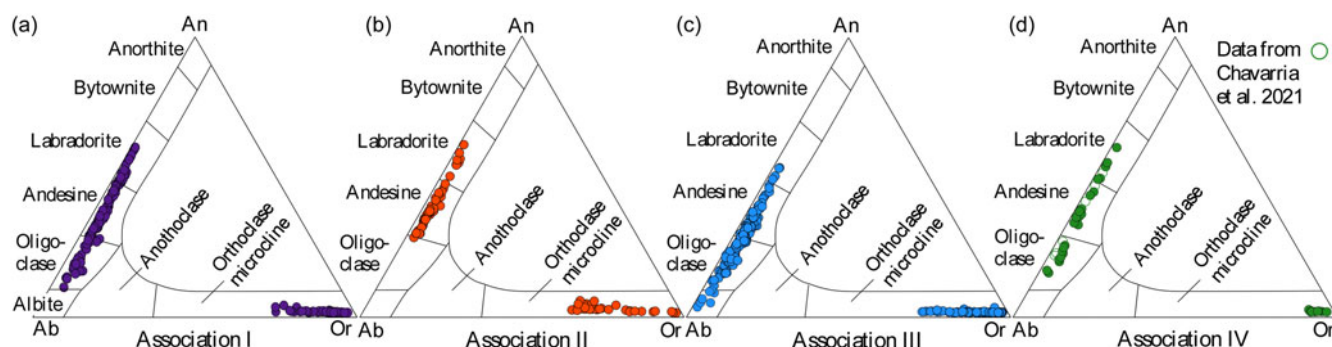
Figure 5. (Colour online) Anorthite (An) – Albite (Ab) – Orthoclase (Or) molecular ternary plot (Deer *et al.*, 2013) for feldspar crystals from the petrographic associations I (a), II (b), III (c), and IV (d) from the Jurassic arc-related plutonic occurrences in southern Colombia.

minerals, with their corresponding structural formulae (see Supplementary Table S3). Additionally, for the purpose of discussion, we have included plagioclase and amphibole chemical data published by Chavarría *et al.* (2021) on the same sample of the Payande Stock from the Southern SCC magma series. The analyzed minerals exhibit significant compositional variations among the four petrographic associations, which we describe in the following.

4.b.1. Feldspars

Plagioclase in all facies exhibits significant compositional variations, with common labradorite-andesine in the cores transitioning to oligoclase-albite compositions at the rims, as depicted in the An–Ab–Or ternary diagram (Fig. 5). As expected, the evolutionary trends are more pronounced in Associations I and III, where anorthite (An) contents range from $An_{57.5-12}$ and $An_{46-1.3}$, respectively. In Association II, the An contents range from $An_{60.8-24.5}$, while in Association IV, they range from $An_{59.8-14.5}$. Moreover, there are significant differences in the orthoclase (Or) content. Associations III and II display the highest Or values, up to 10.4 and 7.9, respectively, while I and IV have Or values up to 1.1 and 1.5, respectively, which indicate contrasted intensive parameters during their crystallization. Among the studied facies, the K-feldspar crystals exhibit relatively homogenous compositions in the Associations I, II and III, being K-rich in IV with Or content ranges of $Or_{97.6-59.5}$, $Or_{98.4-62.8}$, $Or_{97.8-52.5}$ and $Or_{93.7-91.1}$, respectively, see Table S3a.

4.b.2. Pyroxenes

The compositions of pyroxenes found in Associations I and II are illustrated on the Wo–En–Fs quadrilateral diagram in Fig. 6a. The orthopyroxene corresponds to ferroan enstatite, exhibiting average enstatite (En) contents of En_{52} and En_{56} (Table S3b). The clinopyroxenes mainly fall into the calcic Mg-rich augite compositional field, with average compositions of $Wo_{40}En_{39}Fe_{18}$ in I and $Wo_{43}En_{38}Fe_{17}$ in II. Of note, ferroan diopside compositions are prevalent in crystal rims, ranging from $Wo_{45}En_{41}Fe_{12}$ in the monzodiorite facies to $Wo_{46}En_{31}Fe_{20}$ in the quartz monzodiorite facies of Association I. A single data point, obtained over the thickest exsolution lamellae observed, corresponds to an Mg-rich pigeonite (Fig. 6a and Table S3b). In the case of the two-pyroxene-bearing quartz monzodiorites from Association I, the Mg# $[=Mg/(Mg+Fe_T)]$ values of the clinopyroxenes are distinctively higher than those measured for the orthopyroxene (Fig. 6a), with the exception of one analysis with low analytical precision (e.g. low CaO wt %), derived from an
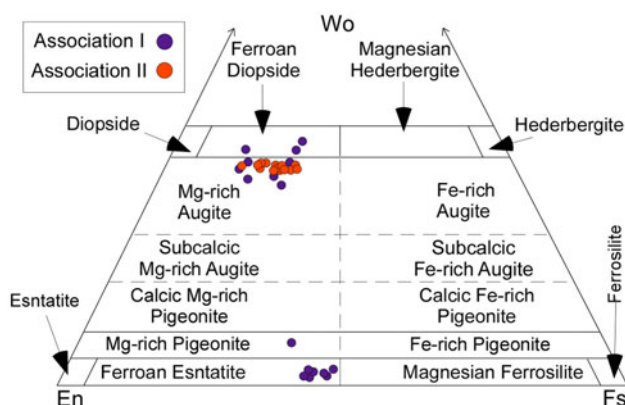

Figure 6. (Colour online) Composition of pyroxene crystals from the Jurassic arc-related plutonic occurrences in southern Colombia: (a) Ferrosilite (Fs) – Wollastonite (Wo) – Enstatite (En) molecular ternary plot (Rock, 1990).

exsolution intergrowth of clinopyroxene into an orthopyroxene crystal (Table S3b).

4.b.3. Amphiboles

The amphiboles in all the studied plutons are calcic ($0.83 \leq {}^BCa/{}^B(Ca + Na) \leq 0.98$) and exhibit significant compositional variations among the different petrographic facies (Table S3c). Accordingly, ferro-ferri-hornblende and magnesium-ferri-hornblende occur in all petrographic facies, while Ti-rich-ferri-tschermakite along with ferri-tschermakite, with the lower alkali contents, and magnesium-hastingsite occur mainly in the Associations IV and III, respectively. The post-magmatic amphibole in Association IV is an actinolite (Fig. 7a). These amphiboles exhibit a strong negative correlation between Al_T and $Si + {}^C(Mg + Fe^{2+})$ and between ${}^{iv}Al + (Na + K)$ and $Si + {}^A[\ ]$ (vacancy in the A site), indicating contributions of both the pressure-sensitive Tschermak and the temperature-sensitive edenite exchanges (Fig. 7b,c; see also Gilbert *et al.* 1982; Holland and Blundy, 1994). In Association IV, the diorite facies show the highest Al_T contents among the studied rocks, reaching up to 2.2 apfu. In comparison, the granodiorite and monzogranite facies have lower values up to 1.6 apfu. In contrast, Associations I, II and III, display intermediate to low Al_T contents, ranging up to 1.8, 1.4 and 0.7 apfu, respectively (Table S3c). Primary amphiboles have average mg# $[=Mg/(Mg+Fe^{2+})]$ numbers of ~0.55 in Association
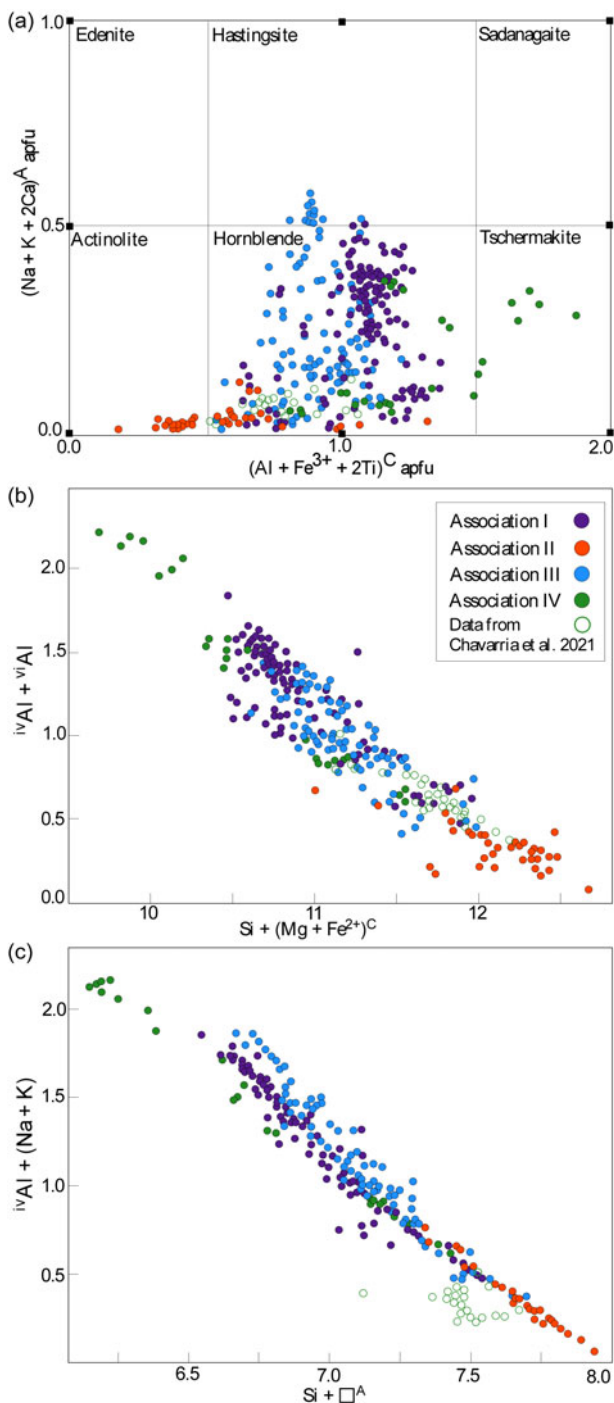
Figure 7. (Colour online) Main compositional variations (apfu) of amphiboles from the Jurassic arc-related plutonic occurrences in southern Colombia: (a) Classification diagram according to Hawthorne *et al.* (2012); (b) Cationic $^{iv}Al + {}^{vi}Al$ vs. $Si + Mg + Fe^{2+}$)^C plot indicating the Al-Tschermak exchange. (c) $^{iv}Al + (Na + K)$ vs. $Si + [\ ]^A$ plot showing the edenite-type exchange (Gilbert *et al.*, 1982; Holland and Blundy, 1994).

I, ~0.62 in Association II, ~0.64 in Association III and ~0.63 in Association IV (Table S3c).

4.b.4. Biotite
The biotite crystals analysed in this study were initially classified using the ternary $10^*TiO_2 - MgO - FeO_T + MnO$ diagram
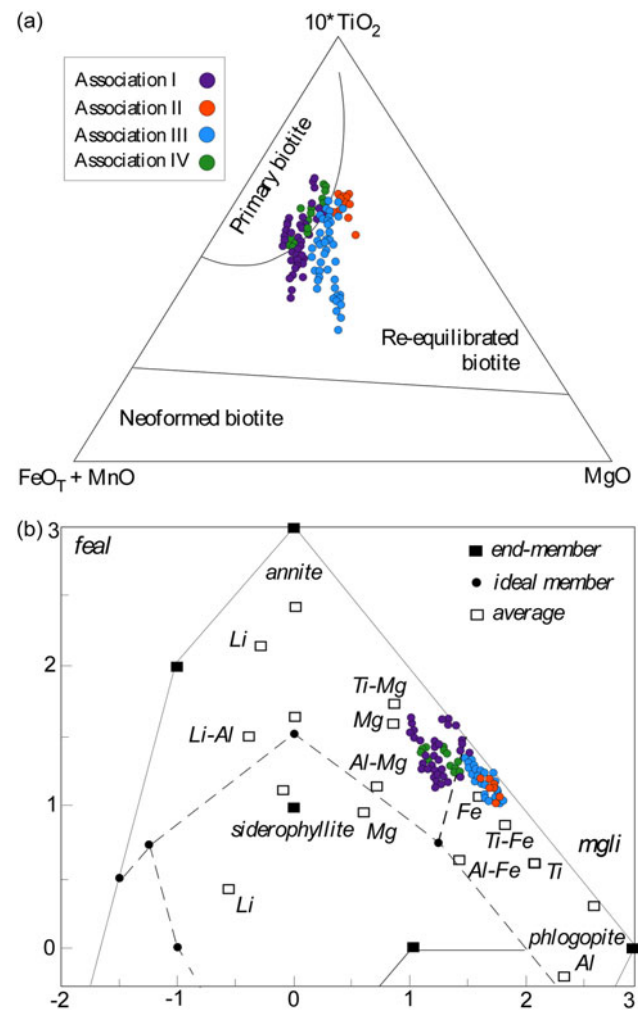

Figure 8. (Colour online) Composition of biotite from the Jurassic arc-related plutonic occurrences in southern Colombia: (a) $10^*TiO2 - FeO - MgO$ ternary diagram (Nachit *et al.*, 2005); (b) Classification feal (Fe$_T$ + Mn + Ti - ^{vi}Al) vs. *mgli* (Mg - Li) diagram according to Tischendorf *et al.* (2007).

proposed by Nachit *et al.* (2005) to distinguish between primary, re-equilibrate (primary biotite modified by hydrothermal fluids) and secondary biotite. According to this classification, the compositions of biotite in most facies of Associations I and IV plot within the primary magmatic biotite field. In the granodiorite facies of Association I, and in all plutonic facies of Associations II and III, biotite crystals are predominantly re-equilibrated (Fig. 8a). These findings are consistent with the observed textural relationships, where re-equilibrated biotite crystals commonly display varying degrees of hydrothermal alteration (Figs. 3 and 4). Figure 8b depicts the *feal vs mgli* classification diagram proposed by Tischendorf *et al.* (2007). In this diagram, the primary biotite crystals are classified as Mg-rich annite. They have average mg# [$=Mg/(Mg+Fe^{2+})$] numbers and Al$_T$ (apfu) contents of ~0.48 and ~1.35 in Association I, and ~0.51 and ~1.26 in Association IV, respectively. On the other hand, re-equilibrated biotite is predominantly represented by Fe-rich phlogopite (Fig. 8b). These types show average mg# and Al$_T$ (apfu) contents of ~0.43 and ~1.39 in Association I, ~0.66 and ~1.16 in II and ~0.60 and ~1.19 in III, respectively (Table S3d).

5. Discussion

5.a. Estimation of physicochemical crystallization conditions

Using the available thermobarometric models and the obtained compositions for clinopyroxene and amphibole, we were able to estimate the prevailing temperatures, pressures, oxygen fugacities and the water contents of the crystallization environments related to each of the studied plutons. These constraints are crucial for understanding the processes that control magma generation and evolution and for reconstructing the thermal and emplacement history of the Jurassic plutonic rocks exposed in southern Colombia. The results (average values) are summarized in Table 2; the full dataset is listed in supplementary Tables S2b and S2c.

5.a.1. Temperature

Petrographic observations have indicated that clinopyroxene is an early-crystallized phase found exclusively in the monzodiorite, quartz monzodiorite and quartz monzonite facies of Associations I and II from UMV. Therefore, by measuring the crystallization temperature of clinopyroxene, it is possible to estimate the near-liquidus temperature of the parental magmas for the corresponding magma series. The model proposed by Wang *et al.* (2021), unlike other thermometers that rely on additional information from melt compositions or coexisting minerals (e.g. Liang *et al.* 2013; Putirka *et al.* 1996; Putirka, 2008), depends solely on the clinopyroxene compositions and the resulting temperatures appear to be more accurate on the average, as evidenced by comparisons in Wieser *et al.* (2023). In our calculations, we assumed an average H_2O content in the melt of ~4.0 wt %, according to the broadly estimated water contents in mafic arc magmas (Plank *et al.* 2013). The estimated clinopyroxene temperatures in both associations overlap but are higher on average for the monzodiorite and quartz monzodiorite rocks of Association I (970°C–1087°C) as compared to those quartz monzodiorites and monzonites of Association II (988°C–1011°C) see Table 2. Considering that clinopyroxenes were among the first crystallized mineral phases, these results are interpreted to represent thermal conditions near the liquidus of the older magmas within the UMV domain.

The amphibole-plagioclase thermometer developed by Holland and Blundy (1994) is a widely accepted model for estimating the close-to-solidus crystallization temperatures of hydrous magmas within arc magmatic systems. In our study, the criteria for its application have been consistently met in all investigated plutonic rock samples, defined by the typical mineral assemblage of quartz + plagioclase + K-feldspar + hornblende + biotite + titanite + magnetite + apatite. For comparison, the new Ti-Amp thermometer of Liao *et al.* (2021), which is based on the titanium content of calcic amphibole-bearing igneous and high-grade metamorphic rocks, was also applied in this study.

We obtained variable crystallization temperatures for the distinct plutons in which mostly diorite, monzodiorites and quartz monzodiorites facies record higher T conditions relative to quartz monzonites, granodiorites and granites. Temperatures determined by the plagioclase-hornblende thermometer in the plutonic occurrences constituted by Association IV display the highest temperatures, ranging from 691°C to 761°C (±40), followed by Association I and III, with temperatures between 656°C–747°C (±40) and 655°C–708°C (±40), respectively. In contrast, Association II results in the lowest temperatures range from 647°C to 673°C (±40). Regarding the amphibole-only

thermometer, the calculated crystallization temperatures are mostly consistent with those mentioned above, with plutons in Association IV yielding 671°C–873°C (±35), Association I 656°C–766°C (±35) and Association III 601°C–691°C (±35), except for samples in Association II, which exhibit considerable underestimations about the close-to-solidus temperature conditions between 467°C and 517°C (±35). Of note, there are underestimations in specific samples from Associations I and III from the obtained temperatures by using the model of Liao *et al.* (2021), as evidenced by the greater standard deviations of the data compared to those obtained using the Holland and Blundy (1994) model (see Supplementary Table S4). Therefore, we opted to show only the plagioclase-hornblende temperature estimations in Table 2 and Fig. 9a.

Differences in temperature crystallization conditions among the four association groups can be attributed to variations in the magmatic processes and/or the degree of fractionation that occurred in each plutonic body. They may suggest that the entire Jurassic plutonic arc magmatic system in southern Colombia underwent distinct thermal histories, which influenced the observed contrasting mineral compositions and textures. In the case of the clinopyroxene-bearing rocks, the amphibole-derived temperatures are in general agreement with those clinopyroxene-derived, as amphibole was relatively late in the crystallization sequence; however, in the case of Association II, the amphibole temperatures are significantly lower approaching the expected close-to-solidus temperatures, and the resulting temperature gap is much large (up to *c.* 300°C), suggesting amphibole late re-equilibration. On the other hand, thermal conditions recorded by the amphibole-bearing rocks, in which amphibole crystallized at intervals above the solidus temperatures ranging between ≥700°C and ≤800°C, in general, suggest an early crystallization stage of this phase in the mineral sequences of Associations I and IV. In this sense, when compared to the zircon saturation temperatures recorded by these rocks (with mean values of 718°C, Table 1; see also Chavarría *et al.* 2021), zircon appears to be a relatively late magmatic phase in the crystallization history of the more evolved granites in the studied region.

5.a.2 Pressure

We also used the model by Wang *et al.* (2021) to determine the crystallization pressures of the clinopyroxenes. However, we found limitations in the case of the monzonite facies in Association II due to the relatively high uncertainty errors associated with its clinopyroxene compositions. Nevertheless, reliable crystallization pressures were computed for the clinopyroxene-bearing monzodiorite and quartz monzodiorite facies of Association I. The zoned clinopyroxene in the monzodiorite facies from the Paez Massif indicates high pressures of ~6.3 kbar for the augite cores and low pressures of ~2.5 kbar for the diopside rims (Table 2). The observed pressure differences between the core and rim zones in the Paez Massif may be attributed to magma crystallization under deeper conditions in an initial stage, followed by magma ascending to a shallower magma chamber while fractionating, as expected in natural magmatic plumbing systems. As for clinopyroxenes in the quartz monzodiorite facies from the Sombrerillo Batholith, we obtained a lower pressure of 1.6 (±1.6) kbar relative to the Paez monzodiorite rock (Table S3c). However, this result should be interpreted with caution, as the analysed clinopyroxene crystals are overgrown by hornblende, forming the typical corona textures in this rock (Fig. 3). In fact, a relatively higher pressure was derived

Table 2. Estimated mean values of crystallization physicochemical parameters of the studied Jurassic arc-related plutonic occurrences

Petrographic association	Occurrence	Sample	Facies	T1 (°C) (±36°)	T2 (°C) (±40°)	P1 (kbar) (±1.6)	P2 (kbar) (±0.5)	Depth from P2 (km)	Physico-chemical conditions logf_{O_2} (±0.3)	Δ NNO	H_2O (±14%)
I (UMV)	Paez Massif	JR1	Monzodiorites	1087–1066	656	6.3–2.5	1.3	4.9	–	–	–
		JR2		–	678	–	2.9	11.2	−12.9	0.8	6.6
		JR3	Qz monzodiorite	–	698	–	2.9	11.2	−14.1	0.2	6.6
	Sombrerillo Batholith	JR5	Quartz monzodiorites	1013	747	–	2.2	8.5	−13.6	1.2	5.9
		JR6		970	731	–	2.5	9.3	−14.3	0.4	4.9
		JR8	Granodiorite	–	699	–	3.1	11.6	–	–	–
	Minas Pluton	JR9	Monzodiorite	–	671	–	2.1	8.1	−15.0	−0.1	5.8
II (UMV)	Astilleros Pluton	JR10	Quartz monzodiorites	–	656	–	1.0	3.6	−15.8	1.2	–
		JR11		1004	647	–	0.9	3.5	–	–	–
	Naranjos Pluton	JR12	Quartz monzonites	996	–	–	–	–	–	–	–
	Anchique Stock	JR13		–	673	–	0.9	3.3	−15.3	1.3	–
		JR14		1011	664	–	0.7	2.7	–	–	–
	San Cayetano Stock	JR-15		988							
III (UMV)	Mocoa Batholith	JR16	Granites		672		1.7	6.4	−13.6	0.1	3.9
	Algeciras Massif	JR17			667		2.0	7.6	−12.9	1.0	4.9
		JR18			708		2.8	10.6	−13.1	1.2	5.7
		JR19			689		2.0	7.7	−12.9	1.4	4.9
		JR20			684		1.9	7.3	−12.9	1.1	4.5
	Altamira Massif	JR23	Granodiorite		673		1.9	7.0	−12.6	0.8	4.0
		JR24	Granites		681		1.8	7.0	−14.1	0.7	5.1
		JR25			655		1.5	5.5	−14.3	0.4	4.9
IV (SCC)	Southern Ibague Batholith	JR26	Diorite		761		3.9	15.0	−13.7	−0.8	6.1
		JR27	Monzogranite		748		2.0	7.7	−14.4	−0.6	4.9
	Payande Stock	JR28	Granodiorite		691		1.1	4.3	−16.2	−0.7	–

Thermobarometry calculations based on: T1 and P1 = Cpx-thermobarometry calibrations by Wang *et al.* (2021); T2 = amphibole-plagioclase thermometer by Holland and Blundy (1994) (expression B); P2 = Al-in-hornblende barometer by Mutch *et al.* (2016); Depths were determined based on pressure conditions, assuming an equivalent 3.8 km pressure gradient for the average crustal density of 2.7 g cm⁻³; Physico-chemical conditions of magmas (logf_{O_2}, H_2Omelt) according to amphibole-only calibrations by Ridolfi (2021).
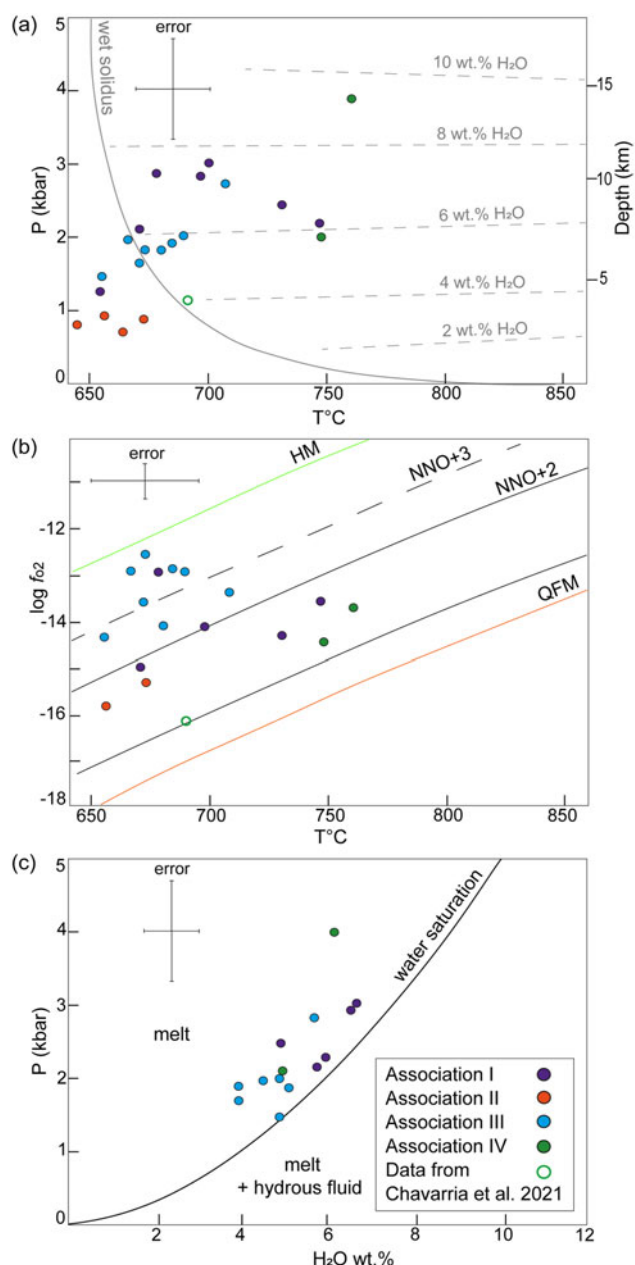
Figure 9. (Colour online) Crystallization conditions for the distinctive petrographic facies associations of the Jurassic arc-related plutonic occurrences in southern Colombia: (a) Temperature vs pressure vs depth diagram. Dotted curves correspond to the H_2O contents necessary for water saturation of the melt taken from Holtz *et al.* (1995); (b) logfO_2 vs. temperature showing the Ni-NiO (NNO) and QFM (Quartz-Fayalite-Magnetite) buffers for amphibole compositions from Ridolfi *et al.* (2010); (c) Pressure dependence of H_2O solubility diagram at 800°C after Holtz *et al.* (1995).

from amphibole thermobarometry for this plutonic facies, as we described below.

By using the selected amphibole–plagioclase pairs, we estimated the pressure conditions at which these mineral phases coexist during the crystallization evolution of the plutons employing the barometer developed by Molina *et al.* (2015). Empirical and experimental studies have demonstrated that the Al-in-horn-blende barometer is a reliable tool for estimating the pressure of calc-alkaline igneous rocks (Hammarstrom and Zen, 1986; Schmidt, 1992; Anderson and Smith, 1995; Mutch *et al.* 2016).

Among the classical models, the Al-in amphibole barometer revisited by Mutch *et al.* (2016) incorporates a wider range of mineralogical and chemical variables, leading to comprehensive and reliable pressure estimations. This model has lower uncertainty values and better accuracy at higher pressures. Therefore, we compare the model of Mutch *et al.* (2016) with the one presented by Molina *et al.* (2015), considering its applicability to our samples, characterized by a mineral assemblage of hornblende + plagioclase (An_{10-60}) + biotite + Fe–Ti oxides + titanite + apatite + alkali feldspar + quartz. The calculated crystallization pressures generally align between the two barometric models, although higher-P values were predominantly obtained with the amphibole–plagioclase pairs compared to the amphibole-only calibration (see Supplementary Table S4). We primarily considered the pressure values obtained with the amphibole-only barometer of Mutch *et al.* (2016) in Table 2 and Figure 9, given their overall accuracy and systematic results across all investigated samples.

Association IV in the SCC domain exhibits the highest and most contrasted pressures of 3.9–2.8 (±0.5–1.5) kbar for the diorite facies and 2.0–1.1 (±0.5–1.5) kbar for the granodiorite and monzogranites (Table 2). For plutons in the UMV domain, Association I shows variable values with pressure values ranging from 3.6–2.2 (±0.5–1.5) kbar in monzodiorite, quartz monzodiorites and granodiorites to 1.3 (±0.5) kbar for a monzodiorite rock. Association III presents similar pressure conditions among all granodiorite and granitic facies with values between 2.8 and 1.5 (±0.5–1.5) kbar. Finally, quartz monzodiorites and quartz monzonites in Association II yielded the lowest pressure conditions of 1.0–0.7 (±0.5) kbar (Table 2). Figure 9a shows a partial positive correlation between the calculated amphibole crystallization temperatures and pressure conditions. As for above, the differences in the estimated pressures, particularly from the Paez Massif and Southern Ibague Batholith, may be compatible with the evolution of magma series at different crustal levels within the plumbing systems and suggest late-fractionation processes during the full solidification of these plutonic rocks in the southern Colombian region.

The obtained crystallization pressures were converted to emplacement depths for each studied occurrence considering an average density of 2.7 g cm^{-3} for the crustal column, and the results are listed in Table 2. Overall, plutonic occurrences from the UMV domain including Association I had emplacement depths ranging from 12–8 km (Sombrerillo Batholith), 11–5 km (Paes Massif) and 8 km (Minas Pluton). Association III has estimated depths ranging from 10–7 km (Algeciras Massif) to 6 km and 7–5 km (Mocoa Batholith and Altamira Massif, respectively). Lastly, the smaller occurrences in Association II (Astilleros and Anchique stocks) were estimated to have emplacement depths of around 3 km (Table 2). As for the plutons in the SCC domain grouped in Association IV, the estimated emplacement depths range from 15–8 km (Southern Ibague Batholith) to 4 km (Payande Stock; Chavarría *et al.* (2021). Of note, Chavarria *et al.* (2021) reported generally high pressures, up to 6.7 kbar and emplacement depths of 25 km, from amphiboles in tonalite/granodiorite facies from the Northern Ibague Batholith, located within the SCC tectonic domain, in the northernmost part of the study area.

5.a.3. Oxygen fugacity (f_{O2}) and water contents (H_2O_{melt})
Oxygen fugacity and water concentration are important parameters that significantly influence the generation, storage and

differentiation of subduction-related magmas (Sisson and Grove, 1993; Stolper and Newman, 1994; Parkinson and Arculus, 1999; Kelley and Cottrell, 2009; Zimmer *et al.* 2010; Grocke *et al.* 2016; Waters and Lange, 2016). To constraint these parameters in our cases, we used the updated experimental calibrations of Ridolfi (2021), following the works of Ridolfi *et al.* (2010) and Ridolfi and Renzulli (2012), which provide the amphibole-only control on log f_{O2} and wt % H_2O in melt for calc-alkaline magmas.

The compositions of magmatic amphiboles from the Jurassic plutons with mg# > 0.50 suggest a primary oxidized crystallization environment for the parental magmas, close to or above the Ni-NiO (NNO) buffer, considering the previously estimated crystallization temperatures (Fig. 9b). Significant differences are observed for some among the studied rocks in both the UMV and SCC domains. On average, amphibole compositions from Association III exhibit the highest log f_{O2} oxidation conditions, ranging between −12 and −14 (ΔNNO = +0.1 to +1.4). Associations I and II record average log f_{O2} values of −12 to −15 (−0.1 ≤ ΔNNO ≤ +1.3) for their amphibole compositions. By contrast, the occurrences of Association IV show the lowest oxygen fugacity conditions in the two studied tectonic domains, with log f_{O2} values ranging from −13 to −16 (−0.8 ≤ ΔNNO ≤ −0.7; Table 2).

Overall, these estimates are compatible with the observed mineral assemblages and the titanite–magnetite–quartz–amphibole–ilmenite buffer (Wones, 1989; Anderson *et al.* 2008) as expected (Table S2), as well as with the relatively high redox conditions deduced from clinopyroxene compositions (cf. Fig. 6b). The Mg-rich compositions of primary biotite and the abundance of magnetite among the Fe–Ti oxides further support the conclusion that the studied rocks were formed under relatively oxidizing conditions, similar to the crystallization systems of granitic rocks of the magnetite series (Ishihara, 1977).

Finally, we obtained a wide range of water concentrations from 3.7 to 8.2 wt % H_2O in the amphibole-precipitation melts from the study plutons. Amphiboles from the diorite, monzodiorite and quartz monzodiorite rocks recorded the highest H_2O wt % values relative to the granites (Supplementary Table S3c). However, some water estimates from the mafic rocks fell outside the thermal stability field of Ridolfi's model. To validate our results, in Fig. 9a, we compared the pressure estimated with experimentally reported water solubility curves for granitic melts proposed by Holtz and Johannes (1994). After assessment, we observed that water estimations between 7 and 8 wt % from the shallower monzodiorite, quartz monzodiorite and quartz monzonite plutons in Associations I and II, respectively, are inconsistent with experimental evidence, resulting in significant overestimations. Therefore, they were not considered for discussion purposes. Data filtering is presented in Fig. 9c, showing H_2O concentrations of 6.6–4.9 wt % in plutons from Association I, 6.1–4.9 wt % in Association IV and 5.7–3.9 wt % H_2O in Association III (Table 2). Our results indicate the presence of highly hydrous melts within the Jurassic arc magmatic system, with H_2O concentrations of ~5.38 wt %.

5.b. Plutonic evolution and implications for the Jurassic magmatic arc in southern Colombia

The physicochemical conditions and observed textural and compositional variations of minerals within the studied occurrences provide valuable insights into the petrogenetic processes that controlled the magmatic history and differentiation of the Jurassic arc in southern Colombia. In particular, the estimated crystallization parameters indicate that plutons within the UMV and SCC domains were formed in distinct magma reservoirs, where fractionation processes occurred at multiple crustal depths along the arc plutonic system, arguably related to different plumbing systems.

The differences in the emplacement depths between these domains can be explained by internal structural controls, in which the regional fault systems (Fig. 2) that extend along the region seem to be separating the UMV and SCC crustal blocks. In this section, we provide a broad understanding of the tectono-magmatic evolutionary history during the construction of the Jurassic arc by integrating the available field observations, whole-rock elemental and isotopic compositions and U-Pb zircon crystallization ages of the studied plutonic occurrences with the acquired mineral compositions and related thermobarometry. Additionally, for comparison, we illustrated the mineral compositional evolutionary paths observed of the main rock-forming phases in terms of Mg# and An parameters, as shown in Fig. 10.

Magma generation in the UMV domain has been linked to a tectonic episode of crustal thickening during the early phase subduction that occurred between 190 and 180 Ma and resulted in the development of an arc crustal column of about ~40 to 50 km paleodepth (Chavarría *et al.* 2021). We propose that in this scenario of thick crust, the massive influx of magma prompted the partial melting of ancient Precambrian rocks at relatively high pressures, causing the generation of high-K (up to 5.3 wt % K_2O, cf. Table 1) metaluminous calc-alkaline magmas within a well-defined MASH zone (melting, assimilation, storage, homogenization; Hildreth and Moorbath, 1988) found in this older magmatic episode. It is argued that the estimated high-pressure crystallization of clinopyroxene (~6 kbar) from the more primitive monzodiorite rock in Association I (Table 2) reflects the initial fractionation of its deep MASH zone as illustrated in Fig. 11. Therefore, we hypothesize that crustal assimilation and/or magma mixing processes played significant roles in the differentiation of the UMV magmas.

The constraints on magma reservoir conditions, derived from the amphibole compositions, indicated that UMV magmas appeared to be relatively oxidized and enriched in water content (Fig. 9 and Table 2). The subsequent fractional crystallization of these magmas resulted in the differentiation of the three distinct Associations I, II and III, under varying high to low pressure and temperature conditions, with emplacement depths ranging from mid- to upper-crustal levels along the arc column. During magma ascent, UMV melts likely incorporated significant crustal materials as suggested by the heterogeneous positive and negative Hf isotopic compositions from plutons in Association III (Garcia, unpub. PhD thesis, São Paulo Univ. Brazil, 2018), the presence of inherited Neoproterozoic zircons in plutons of Association III (Rodríguez *et al.* 2018), unradiogenic Nd isotopic values of most of the arc-related rocks in the region (Leal-Mejía *et al.* 2019) and elevated concentrations of large ion lithophile elements (LILEs) and rare earth elements (REEs), reaching up to 2186 and 265 ppm, respectively, within all UMV plutonic rocks (Table 1). The presence of Precambrian metamorphic rocks and Paleozoic sediments in the region (Gomez *et al.* 2019; Ibañez-Mejia, 2020) suggests the availability of fertile lithologies that can undergo partial melting within the lower crust, especially when mantle-derived magmas are emplaced into the crust.

Evidence of the magma mixing process during the formation of the UMV plutons include the widespread occurrence of microgranular mafic (dioritic) enclaves (Table S2) and related mafic and
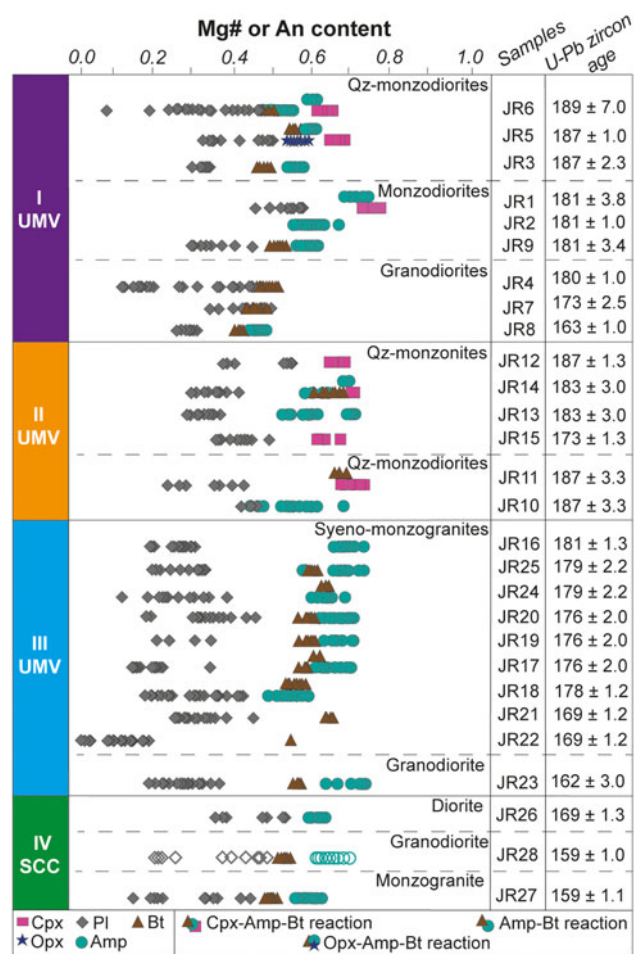
Figure 10. (Colour online) Summary of Mg# numbers of clinopyrox-ene, orthopyrox-ene, amphibole, biotite and An content of plagioclase for the analyzed samples and their reported zircon U-Pb ages of Jurassic arc-related plutonic occurrences in southern Colombia. Of note, unfilled symbols correspond to plagioclase and amphibole data from Chavarría *et al.* (2021).

felsic syn-plutonic dikes from field observations (e.g. García-Chinchilla and Vlach, 2019; Rodríguez-García *et al.* 2020a). The corona and sieve textures observed in ortho- and/or clinopyrox-enes, showing partial replacement by amphibole or biotite (Figs. 3, 8a and 10) are also potential indicators of magma reservoirs undergoing magma mixing/mingling processes (Baxter and Feely, 2002; Kamacı and Altunkaynak, 2019; Schaaf *et al.* 2021; Koua *et al.* 2022; Sousa *et al.* 2022). Additionally, the changing magmatic conditions recorded in the compositional zoning of clinopyroxenes and amphiboles in Associations I and III likely suggest the replenishment of magma batches into pre-existing magma reservoirs, leading to disequilibrium conditions and mixing processes during the crystallization of primitive UMV magmas. Based on the petrological features described above, along with the similar geochemical trace element compositions (Table 1) and coexisting fractionation patterns observed in the different mafic and felsic rocks from the UMV domain (see Rodríguez *et al.* 2018), we argue that the mixing/mingling of magmas might serve as a complementary petrological process in the lower crust MASH zone, contributing to the magmatic evolutionary history of the UMV rocks. This process may potentially explain the wide variability of the plutonic rocks in the region. However, to fully evaluate the specific contributions of the role of mixing and/or

crustal assimilation, further investigations should employ geo-chemical and isotopic models.

During the first interval of magmatic evolution from *c.* 195 to 183 Ma, mineral chemistry results reveal the significant role of clinopyroxene, fractionating at different pressures between 6 and 2 kbar (Table 2), in driving the differentiation of early-formed monzodiorite, quartz monzodiorite (Association I) and monzonite and quartz monzonite (Association II) rocks. The observed evolutionary trends in these rocks include the extensive crystal-lization of clinopyroxene with a range of Mg# values from 0.78 to 0.53, plagioclase with varying An_{57-12} contents and the subsequent crystallization of Mg-rich amphiboles (Mg# = 0.75–0.44; Fig. 10). Crystallization of Mg-rich annite with Mg# evolutionary trends from 0.57 to 0.41 record the next stage of solidification of the early UMV magmas in the arc system. Moreover, this early magmatism is notably characterized by distinct intrusion events of Association I and II intrusions at mid- to upper-crustal depths, as previously estimated. Considering the established steady-state scenario that characterized the onset of subduction-driven magmatism within this Jurassic arc (Bustamante *et al.* 2019), we can only speculate about the existence of localized structural heterogeneities within the arc crustal column. These variations in the stress regime might have facilitated the continuous ascent of less voluminous magmas along vertically arc-parallel faults, such as the Agrado-Betania and Fraile-Pava faults, depicted in Fig. 2. Consequently, smaller, and relatively more, homogeneous intrusions and stocks like those grouped in Association II were emplaced at shallower crustal levels in the central UMV region (Fig. 11). This hypothesis gains support from the spatial relationships observed, where Association II bodies intruded the volcanic sequences of the Saldaña Formation, representative of the primary component of the arc volcanic front within the Jurassic magmatic system.

Between ~180 and 165 Ma, the magmas in the UMV domain evolved through plagioclase and amphibole-dominated fractiona-tion, reflected in the compositional trends of An_{46-1} and Mg# 0.74–0.49, respectively (Fig. 10), resulting in the formation of granodiorite and granite rocks (Association III). Of note, the more evolved granites exhibit slight variations in the intensive crystallization parameters, characterized by higher f_{o2} oxidation but lower H_2O_{melt} values when compared to the intermediate rocks of Associations I and II (Fig. 9 and Table 2). These differences are arguably attributed to enhanced crustal assimilation interactions during magma ascent within the plumbing system (Blatter *et al.* 2013; Humphreys *et al.* 2014; Grocke *et al.* 2016). These processes caused the destabilization of the amphibole crystals and the subsequent formation or re-equilibrate biotite, as evidenced in the shallower emplacement plutons of Associations II and III (Figs. 3, 8 and 10). Comparing the crystallization sequences of the UMV plutonic rocks, we have observed overlapping mineral evolutionary trends among contemporaneous granodiorites of Association I and granites of Association III emplaced at ~162 to 163 Ma (Fig. 10). This suggests similar magmatic differentiation trends occurred in both the western and eastern parts of the UMV domain, supporting the idea that the older (~195 to 165 Ma) Jurassic magmatic episode of arc construction in southern Colombia was developed within a stationary subduction setting (Bustamante *et al.* 2019).

Bustamante *et al.* (2016) suggest that the tectonic regime changed to a more oblique subduction setting during the younger (~165 to 145 Ma) Jurassic magmatic episode. This tectonic scenario could have potentially led to the underplating of new mantle-derived melts and the formation of a distinct magma
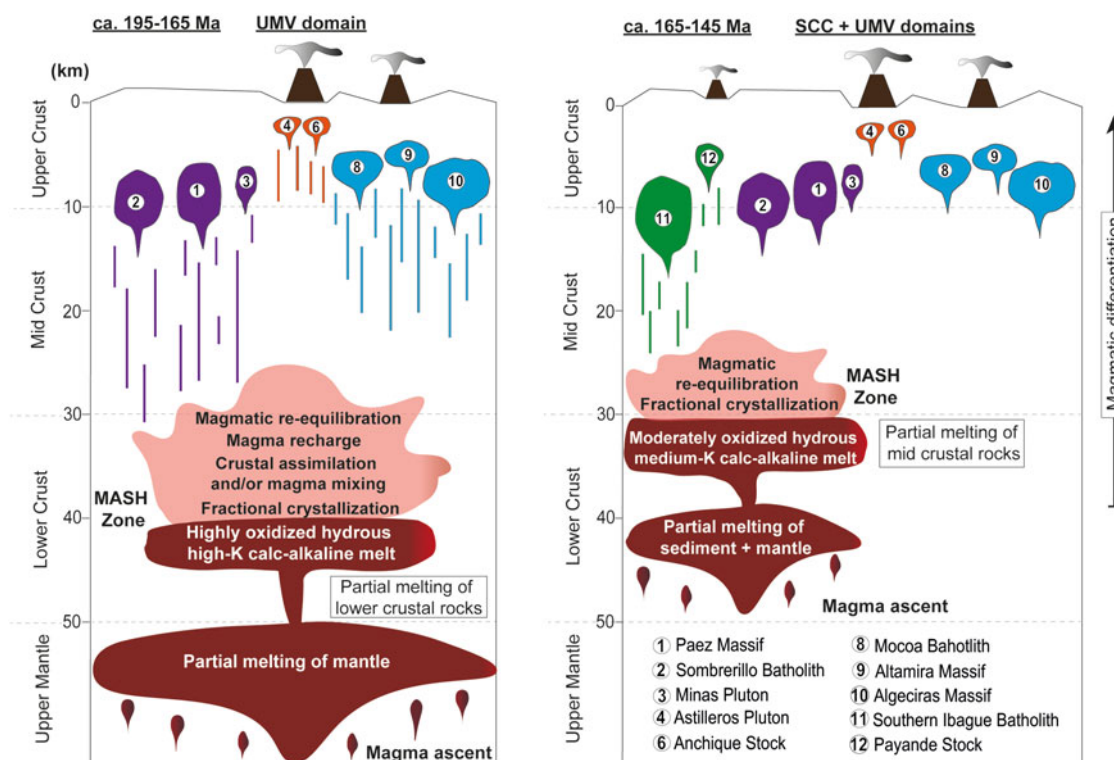
Figure 11. (Colour online) Conceptual approach to the magmatic arc system and processes involved in the Jurassic plutonism in southern Colombia.

reservoir within a thinned crust, at depths of ~25–45 km (Chavarría *et al.* 2021). Isotopic data from Sr, Nd, Pb and Hf compositions consistently indicate an increasingly juvenile signature in the magmatic record between 165 and 129 Ma (Cochrane *et al.* 2014a; Bustamante *et al.* 2016; Quandt *et al.* 2018; Leal-Mejía *et al.* 2019). This is further supported by the distinct redox conditions recorded by the plutonic occurrences of Association IV (Fig. 9 and Table 2). These conditions reflect the addition of less oxidizing slab fluids ascending in the mantle wedge, resulting in the formation of moderately oxidized and hydrous calc-alkaline medium-K magmas (up to 3.9 wt % K$_2$O), with discrete LILEs and REEs concentrations (reaching up to 1197 and 119 ppm, respectively; Table 1). Subsequently, the development of magma fractionation processes within a mid-crustal MASH zone likely led to the crystallization of the younger Jurassic plutons within the SCC domain.

Although the examined samples of Association IV from the Ibague Batholith and Payande Stock in the SCC domain are limited, we were able to identify key aspects that provide insights into the potential magmatic processes involved in the formation of these younger Jurassic plutons. Our mineral chemistry data suggest that SCC magmas have been differentiated by primary fractionation of plagioclase with varying An$_{57-12}$ contents, and amphibole and biotite with Mg# values from 0.69 to 0.54 and 0.54 to 0.58, respectively (Fig. 10). We hypothesize that the diorite facies, with cumulate amphibole + plagioclase texture and crystallized under high pressure, records the accumulation of crystal from the melt at the base of the younger magma chamber. Thermobarometry supports this interpretation, suggesting that this rock likely represents the root of the intrusive Southern Ibague Batholith established at mid-crust levels (Table 2). Previous studies suggest that the formation of this intrusive body in the region involved

multiple intrusions, evidenced by continuous magma pulses from *c.* 171 to 137 Ma (Leal-Mejía *et al.* 2019; Rodríguez-García *et al.* 2022). These multiple injection events are further supported by the contrasting crystallization pressure and temperature conditions of the diorite and monzogranite rocks in the Southern Ibague Batholith, indicating a late magmatic re-equilibration process, as discussed in the previous section. Indeed, the common occurrence of concentric-zoned plagioclase crystals within this association (Figs. 3 and 4) suggests extensive crystal fractionation during the evolution of the SCC magmas. Therefore, we propose that magmatic differentiation may have persisted after the early magma injections, allowing later, more evolved magmas to ascend and reach the uppermost crust. This is supported by the shallower emplacement depths of the granodiorite and monzogranite rocks in the SCC domain (Fig. 11).

5.c. Late Jurassic to Early Cretaceous fragmentation and exhumation of the magmatic arc

Our constraints on the emplacement depth of the Jurassic plutonic rocks from the UMV and SCC domains in southern Colombia have provided minimum exhumation values for several segments of the Jurassic magmatic arc. The inferred paleodepths exhibit a total exhumation pattern that partially aligns with the modern geomorphic provinces of the Northern Andes. The westernmost plutonic basement rocks of the SCC domain exhibit the highest amount of total exhumation of ~15 km, while the eastern basement rocks of the UMV demonstrate total exhumation values ranging from 12 to 5 km, with minor intra-basin exhumation between 2 and 4 km within the UMV. These results support the models suggesting that the Central Cordillera in the SCC domain has undergone more prolonged deformation and exhumation

compared to other provinces in the Northern Andes (Zapata *et al.* 2021).

Six of the investigated occurrences are situated within coherent structural basement blocks overlain by Cretaceous strata, indicating rock exhumation between magma crystallization and sediment deposition. Hence, the inferred paleodepth values presented in this study provide a constraint on the magnitude of deformation during this period. The Late Jurassic to Early Cretaceous exhumation inferred from thermobarometry data includes ~10 km in the Sombrerillo Batholith and the Paez and Algeciras Massifs, ~6 km in the Mocoa Batholith and the Altamira Massif and >4 km in the Astilleros, Anchique and Payande Stocks. The absence of distinct Cretaceous unconformities in the remaining structural blocks domain precludes any inferences about this exhumation event.

This major exhumation event can be correlated to either terrane collision and crustal thickening during the Late Jurassic (Blanco-Quintero *et al.* 2014; Bustamante *et al.* 2016), the onset of crustal extension (Zapata *et al.* 2020) or a combination of both. Detrital zircon fission-track ages obtained from the Cretaceous strata in the Upper Magdalena Basin suggest a Jurassic to Early Cretaceous exhumation event (Calderon-Diaz *et al.* 2024). Nevertheless, these age populations lack the resolution to determine whether this exhumation was triggered by collisional or extensional tectonic processes. A zircon fission-track age derived from the Astilleros Pluton implies that in this specific structural block, exhumation took place around 124 Ma. This finding aligns more closely with exhumation associated with extensional tectonic activity (Valencia-Gómez *et al.* 2024).

Several questions and observations can be addressed based on this dataset. The eastern segment of the Central Cordillera and the Algeciras Massif exhibit higher exhumation values, followed by the Mocoa Batholith, while lower values are observed within the Upper Magdalena Basin. This pattern resembles the modern basin configuration, suggesting a plausible control of these past events on subsequent deformation phases. Moreover, it implies a long-lived deformation history of the fault systems limiting these structural blocks (e.g. La Plata-Chusma, Agrado-Betania and Algeciras Fault systems). In either compressional or extensional tectonics, such amounts of exhumation would have resulted in a substantial sedimentary influx into extensional or flexural basins associated with the exhumed blocks. However, the absence of sedimentary strata from this period remains enigmatic. We present compelling evidence of significant Late Jurassic to Early Cretaceous rock exhumation. Nonetheless, the tectonic precursors, refined spatial-temporal patterns and the absence of associated sedimentation remain as open research questions.

6. Conclusions

Petrographic and mineral chemistry data from representative samples of calc-alkaline I-type plutons in southern Colombia, formed during two main Jurassic magmatic episodes (~195 to 165 and ~165 to 145 Ma) in the Northern Andes, allow significant conclusions regarding their crystallization conditions to be drawn. Coupled with the available geochemical and geochronological data, these results provide a better understanding of the petrogenesis and the regional geological and geomorphological configuration of this region in Colombia.

- The investigated Jurassic plutons can be grouped according to four main distinct petrographic associations each with its proper compositional range. The older occurrences (~195 to 165 Ma) exposed in the UMV domain of the southern Colombian region include monzodiorites, quartz monzo-diorites and granodiorite compositions (I), quartz monzo-diorites and quartz monzonites (II) and granodiorite and granites (III) and crops out as large batholiths, plutons or stocks. The younger occurrences (~165 to 145 Ma) exposed in the SCC domain of the region comprise relatively large and small occurrences made up of diorites, granodiorites and monzogranites.
- The main rock-forming minerals in these plutons exhibit significant compositional variations, which are interpreted to reflect initial magma compositions, contributions acquired from crustal assimilation, magma mixing and fractional crystallization conditions to extents that need further quantitative improvements.
- Constraints in physiochemical conditions indicate that the studied plutons were formed in distinct magma reservoirs. The older Jurassic plutons crystallized from highly oxidized and hydrous mixed mantle-crustal source magmas, while the younger Jurassic plutons were derived from subduction-modified mantle sources with relatively lower oxidation states and hydrous contents.
- The thermobarometry data give new insights into the Jurassic arc-related magmatism in southern Colombia, revealing a heterogeneous crustal architecture. The recorded temperatures and pressures of the Jurassic occurrences range from 669°C to 1051°C and from 0.7 to 6.3 kbar, highlighting significant thermal variations and plutonic emplacement at mid- to upper-crustal levels during the magmatic evolution.
- Emplacement plutonic depths suggest up to 10 km of exhumation between the Late Jurassic and the Early Cretaceous exhumation in southern Colombia, a period where the upper crust deformation is poorly known.

References

Anderson JL and Smith DR (1995) The effects of temperature and fO2 on the Al-in-hornblende barometer. *American Mineralogist* **80**, 549–559.

Anderson JLL, Barth PA, Wooden LJ, Mazdab F, Barth AP, Wooden JL and Mazdab F (2008) Thermometers and thermobarometers in granitic Systems. *Reviews in Mineralogy and Geochemistry* **69**, 121–142.

Bastos VA, Koester E, Lenz C, Dal Olmo-Barbosa L, Porcher CC, Loureiro PO, Vieira DT, Ramos RC and Cedeño DG (2021) Contribution to the understanding of the Pinheiro Machado Complex (Dom Feliciano Belt,

Brazil): a study of textures, mineral chemistry, and crystallization conditions. *Geological Journal* **56**, 1012–1033.

Baxter S and Feely M (2002) Magma mixing and mingling textures in granitoids: examples from the Galway Granite, Connemara, Ireland. *Mineralogy and Petrology* **76**, 63–74.

Bayona G, Bustamante C, Nova G and Salazar-Franco A (2020) Jurassic evolution of the northwestern corner of Gondwana: present knowledge and future challenges in studying Colombian Jurassic rocks. In *The Geology of Colombia, Volume 2 Mesozoic* (eds J. Gómez and D. Mateus–Zabala), pp. 171–207. Servicio Geológico Colombiano, Publicaciones Geológicas Especiales 35, Bogotá.

Blanco-Quintero IF, García-Casco A, Toro LM, Moreno M, Ruiz EC, Vinasco CJ, Cardona A, Lázaro C and Morata D (2014) Late Jurassic terrane collision in the northwestern margin of Gondwana (Cajamarca Complex, eastern flank of the Central Cordillera, Colombia). *International Geology Review* **56**, 1852–1872.

Blatter DL, Sisson TW and Hankins WB (2013) Crystallization of oxidized, moderately hydrous arc basalt at mid- to lower-crustal pressures: implications for andesite genesis. *Contributions to Mineralogy and Petrology* **166**, 861–886.

Blundy J and Cashman K (2008) Petrologic reconstruction of magmatic system variables and processes. *Reviews in Mineralogy and Geochemistry* **69**, 179–239.

Bustamante C and Bustamante A (2019) Two Cretaceous subduction events in the Central Cordillera: insights from the high P–low T metamorphism. In *The Geology of Colombia, Volume 2 Mesozoic* (eds J. Gómez and D. Mateus–Zabala), pp. 485–498. Servicio Geológico Colombiano, Publicaciones Geológicas Especiales 35, Bogotá.

Bustamante C, Cardona A, Bayona G, Mora A, Valencia V, Gehrels G and Vervoort J (2010) U-Pb LA-ICP-MS geochronology and regional correlation of Middle Jurassic intrusive rocks from the Garzon Massif, Upper Magdalena Valley and Central Cordillera, Southern Colombia. *Boletin de Geología* **32**, 93–109.

Bustamante C, Archanjo CJ, Cardona A and Vervoort JD (2016) Late Jurassic to Early Cretaceous plutonism in the Colombian Andes: a record of long-term arc maturity. *Bulletin of the Geological Society of America* **128**, 1762–1779.

Bustamante C, Archanjo CJ, Cardona A, Bustamante A and Valencia VA (2017) U-Pb Ages and Hf Isotopes in zircons from parautochthonous Mesozoic terranes in the Western margin of Pangea: implications for the terrane configurations in the Northern Andes. *Journal of Geology* **125**, 487–500.

Bustamante C, Cardona A, Bustamante A and Vanegas J (2019) Comment on 'Petrotectonic characteristics, geochemistry, and U-Pb geochronology of Jurassic plutons in the Upper Magdalena Valley-Colombia: implications on the evolution of magmatic arcs in the NW Andes' by Rodríguez *et al.* (2018). *Journal of South American Earth Sciences* **95**, 101987.

Bustamante C, Cardona A, Restrepo M, Zapata D, Beltrán-triviño A, Bustamante A, Valencia VA, Bustamante C, Cardona A, Restrepo M, Zapata D and Beltrán-triviño A (2023) Middle Triassic to Jurassic convergence at the north-western margin of Gondwana : insights from the Central Cordillera of Colombia Middle Triassic to Jurassic convergence at the north-western margin of Gondwana : insights from the Central Cordillera of Co. *International Geology Review* **00**, 1–21.

Calderon-Diaz L, Zapata S, Cardona A, Parra M, Sobel ER, Patiño AM, Valencia V, Jaramillo-Rios JS and Glodny J (2024) Cretaceous extensional and contractional stages in the Colombian Andes unraveled by a source-to-sink geochronological and thermochronological study in the Upper Magdalena Basin. *Tectonophysics* **878**, 230303.

Chavarría L, Bustamante C, Cardona A and Bayona G (2021) Quantifying crustal thickness and magmatic temperatures of the Jurassic to Early Cretaceous North-Andean arc. *International Geology Review* **00**, 1–21.

Cobbing EJ and Pitcher WS (1983) Andean plutonism in Peru and its relationship to volcanism and metallogenesis at a segmented plate edge. *Geological Society of America Memoir* **159**, 277–291.

Cochrane R, Spikings R, Gerdes A, Winkler W, Ulianov A, Mora A and Chiaradia M (2014a) Distinguishing between in-situ and accretionary growth of continents along active margins. *Lithos* **202**, 382–394.

Cochrane R, Spikings R, Gerdes A, Ulianov A, Mora A, Villagómez D, Putlitz B and Chiaradia M (2014b) Permo-Triassic anatexis, continental rifting and the disassembly of western Pangaea. *Lithos* **190**, 383–402.

Cui X, Sun M, Zhao G, Zhang Y and Yao J (2021) Two-stage mafic-felsic magma interactions and related magma chamber processes in the arc setting: an example from the enclave-bearing calc-alkaline plutons, Chinese Altai. *Geochemistry, Geophysics, Geosystems* **22**, e2021GC009939.

Deer WA, Howie RA and Zussman J (2013) *An Introduction to the Rock-Forming Minerals.* London: Mineralogical Society, 498 p.

Erdmann S, Martel C, Pichavant M and Kushnir A (2014) Amphibole as an archivist of magmatic crystallization conditions: problems, potential, and implications for inferring magma storage prior to the paroxysmal 2010 eruption of Mount Merapi, Indonesia. *Contributions to Mineralogy and Petrology* **167**, 1–23.

Espitia W, Cortés M, Beltrán W, Higuera Díaz IC and Arias J (2022) Structural styles of the Upper Magdalena valley, Northern Andes, Colombia: case studies. In *Andean Structural Styles*, pp. 139–148. Elsevier.

García-Chinchilla DA and Vlach SRF (2019) Geological mapping of intrusive rocks: a case study in the Garzón region, the Eastern Cordillera of the Colombian Andes. *Geologia USP. Série Científica* **19**, 43–62.

García-Delgado WH, Velandia F, Bermúdez MA and Audemard F (2022) The present-day tectonic regimes of the Colombian Andes and the role of slab geometry in intraplate seismicity. *International Journal of Earth Sciences*. https://doi.org/10.1007/s00531-022-02227-9

Gilbert M, Helz RT, Popp R and Spear F (1982) Experimental studies of amphibole stability. In *Reviews in Mineralogy* (eds D. Veblen and P. Ribbe), pp. 229–353, 9B edition. Mineralogical Society of America.

Gomez J, Schobbenhaus C, Montes N and compilers (2019) Geological Map Of South America At a Scale of 1: 5M. Pris.

Grocke SB, Cottrell E, de Silva S and Kelley KA (2016) The role of crustal and eruptive processes versus source variations in controlling the oxidation state of iron in Central Andean magmas. *Earth and Planetary Science Letters* **440**, 92–104.

Gündüz M and Asan K (2022) MagMin_PT: an Excel-based mineral classification and geothermobarometry program for magmatic rocks. *Mineralogical Magazine* **87**, 1–9.

Hammarstrom JM and Zen E (1986) Aluminum in hornblende: an empirical igneous geobarometer. *American Mineralogist* **71**, 1297–1313.

Hawthorne FC, Oberti R, Harlow GE, Maresch W V, Martin RF, Schumacher JC and Welch MD (2012) Nomenclature of the amphibole supergroup. *American Mineralogist* **97**, 2031–2048.

Hildreth W and Moorbath S (1988) Crustal contributions to arc magmatism in the Andes of Central Chile. *Contributions to Mineralogy and Petrology* **98**, 455–489.

Holland T and Blundy J (1994) Non-ideal interactions in calcic amphiboles and their bearing on amphibole-plagioclase thermometry. *Contributions to Mineralogy and Petrology* **116**, 433–447.

Holtz F, Behrens H, Dingwell DB, Johannes W. 1995. H_2O solubility in haplogranitic melts: compositional, pressure, and temperature dependence. *American Mineralogist.* **80**, 94–108. https://doi.org/10.2138/am-1995-1-210.

Holtz F and Johannes W (1994) Maximum and minimum water contents of granitic melts: implications for chemical and physical properties of ascending magmas. *Lithos* **32**, 149–159.

Humphreys MCS, Brooker RA, Fraser DG, Burgisser A, Mangan MT and McCammon C (2014) Coupled interactions between volatile activity and Fe oxidation state during arc crustal processes. *Journal of Petrology* **56**, 795–814.

Ibañez-Mejia M (2020) The Putumayo orogen of Amazonia: a synthesis. In *The Geology of Colombia, Volume 1 Proterozoic – Paleozoic* (eds J. Gómez and D. Mateus–Zabala), pp. 101–131. Servicio Geológico Colombiano, Publicaciones Geológicas Especiales 35.

Ishihara S (1977) The magnetite-series and ilmenite-series granitic rocks. *Mining geology* **27**, 293–305.

Kamacı Ö and Altunkaynak Ş (2019) Magma chamber processes and dynamics beneath northwestern Anatolia: insights from mineral chemistry and crystal size distributions (CSDs) of the Kepsut volcanic complex (NW Turkey). *Journal of Asian Earth Sciences* **181**, 103889.

Kazemi K, Kananian A, Xiao Y and Sarjoughian F (2018) Chemical composition of rock-forming minerals and crystallization physicochemical

conditions of the Middle Eocene I-type Haji Abad pluton, SW Buin-Zahra, Iran. *Arabian Journal of Geosciences* **11**, 717.

Kelley KA and Cottrell E (2009) Water and the oxidation state of subduction zone magmas. *Science* **325**, 605–607.

Koua KAD, Sun H, Li J, Li H, Xie J, Sun Q, Li Z, Yang H, Zhang L and Mondah OR (2022) Petrogenesis of Early Cretaceous granitoids and mafic enclaves from the Jiaodong Peninsula, eastern China: implications for crust-mantle interaction, tectonic evolution and gold mineralization. *Journal of Asian Earth Sciences* **228**, 105096.

Le Maitre RW, Streckeisen A, Zanettin B, Le Bas MJ, Bonin B, Bateman P, Bellieni G, Dudek A, Efremova S, Keller J, Lameyre J, Sabine PA, Schmid R, SØrensen H, Woolley A. (2002). *Igneous Rocks. A Classification and Glossary of Terms*, 2nd ed. New York: Cambridge University Press. https://doi.org/10.16309/j.cnki.issn.1007-1776.2003.03.004

Leal-Mejía H, Shaw RP and Melgarejo JC (2019) Spatial-temporal migration of granitoid magmatism and the phanerozoic tectono- magmatic evolution of the Colombian Andes. In *Geology and Tectonics of Northwestern South America* (eds F. Cediel and R.P. Shaw), pp. 253–410. Frontiers in Earth Sciences, Springer.

Liang Y, Sun C and Yao L (2013) A REE-in-two-pyroxene thermometer for mafic and ultramafic rocks. *Geochimica et Cosmochimica Acta* **102**, 246–260.

Liao Y, Wei C and Rehman HU (2021) Titanium in calcium amphibole: behavior and thermometry. *American Mineralogist* **106**, 180–191.

de Lima JV, de Pinho Guimarães I, Neves SP, Santos ID, Brainer CCG and Dantas EL (2021) Mineral chemistry constrains on crystallization conditions and petrological evolution of the Teixeira Batholith granitoids, Borborema Province, NE Brazil. *Journal of South American Earth Sciences* **112**, 103577.

Locock AJ (2014) An Excel spreadsheet to classify chemical analyses of amphiboles following the IMA 2012 recommendations. *Computers & Geosciences* **62**, 1–11. Elsevier.

Molina JF, Moreno JA, Castro A, Rodríguez C and Fershtater GB (2015) Calcic amphibole thermobarometry in metamorphic and igneous rocks: new calibrations based on plagioclase/amphibole Al-Si partitioning and amphibole/liquid Mg partitioning. *Lithos* **232**, 286–305.

Molina JF, Cambeses A, Moreno JA, Morales I, Montero P and Bea F (2021) A reassessment of the amphibole-plagioclase NaSi-CaAl exchange thermometer with applications to igneous and high-grade metamorphic rocks. *American Mineralogist* **106**, 782–800.

Montes C, Rodriguez-Corcho AF, Bayona G, Hoyos N, Zapata S and Cardona A (2019) Continental margin response to multiple arc-continent collisions: the northern Andes-Caribbean margin. *Earth-Science Reviews* **198**, 102903.

Mutch EJF, Blundy JD, Tattitch BC, Cooper FJ and Brooker RA (2016) An experimental study of amphibole stability in low-pressure granitic magmas and a revised Al-in-hornblende geobarometer. *Contributions to Mineralogy and Petrology* **171**, 1–27.

Nachit H, Ibhi A, Abia EH and Ben Ohoud M (2005) Discrimation entre biotites magmatiques primaires, biotites rééquilibrées et biotites néoformées. *Comptes Rendus - Geoscience* **337**, 1415–1420.

Parkinson IJ and Arculus RJ (1999) The redox state of subduction zones: insights from arc-peridotites. *Chemical Geology* **160**, 409–423.

Plank T, Kelley KA, Zimmer MM, Hauri EH and Wallace PJ (2013) Why do mafic arc magmas contain ~4wt% water on average? *Earth and Planetary Science Letters* **364**, 168–179.

Putirka K, Johnson M, Kinzler R, Longhi J and Walker D (1996) Thermobarometry of mafic igneous rocks based on clinopyroxene-liquid equilibria, 0-30 kbar. *Contributions to Mineralogy and Petrology* **123**, 92–108.

Putirka KD (2008) Thermometers and barometers for volcanic systems. *Reviews in Mineralogy and Geochemistry* **69**, 61–120.

Quandt D, Trumbull RB, Altenberger U, Cardona A, Romer RL, Bayona G, Ducea M, Valencia V, Vásquez M, Cortes E and Guzman G (2018) The geochemistry and geochronology of Early Jurassic igneous rocks from the Sierra Nevada de Santa Marta, NW Colombia, and tectono-magmatic implications. *Journal of South American Earth Sciences* **86**, 216–230.

Ramírez DA, Correa-Martínez AM, Zapata-Villada JP and Rodríguez G (2020) Tectono-magmatic implications of the Jurassic volcanic and volcanoclastic record of the Santa Marta Massif (Colombia). *Journal of South American Earth Sciences* **104**, 102866.

Ramon JC and Rosero A (2006) Multiphase structural evolution of the western margin of the Girardot subbasin, Upper Magdalena Valley, Colombia. *Journal of South American Earth Sciences* **21**, 493–509.

Restrepo M, Bustamante C, Cardona A, Beltrán-Triviño A, Bustamante A, Chavarría L and Valencia VA (2021) Tectonic implications of the jurassic magmatism and the metamorphic record at the southern Colombian Andes. *Journal of South American Earth Sciences* **111**, 103439.

Restrepo M, Bustamante C, Cardona A, Beltrán-Triviño A and Valencia VA (2023) Geochemistry and geochronology of Permian plutonic rocks at the north-western margin of Gondwana. *Geological Journal* **58**, 2818–2840.

Ridolfi F (2021) Amp-TB2: an updated model for calcic amphibole thermobarometry. *Minerals* **11**, 324.

Ridolfi F and Renzulli A (2012) Calcic amphiboles in calc-alkaline and alkaline magmas: thermobarometric and chemometric empirical equations valid up to 1,130°C and 2.2 GPa. *Contributions to Mineralogy and Petrology* **163**, 877–895.

Ridolfi F, Renzulli A and Puerini M (2010) Stability and chemical equilibrium of amphibole in calc-alkaline magmas: an overview, new thermobarometric formulations and application to subduction-related volcanoes. *Contributions to Mineralogy and Petrology* **160**, 45–66.

Rock NMS (1990) The International Mineralogical Association (IMA/CNMMN) pyroxene nomenclature scheme: computerization and its consequences. *Mineralogy and Petrology* **43**, 99–119.

Rodriguez-Garcia G, Correa-Martinez AM, Zapata-Villada JP and Obando-Erazo G (2019) Fragments of a Permian arc on the western margin of the Neoproterozoic basement of Colombia. In *The Geology of Colombia. Volume 1: Proterozoic - Paleozoic* (eds J. Gómez and D. Mateus–Zabala). Bogotá.

Rodríguez-García G (2018) Caracterización petrográfica, química y edad Ar-Ar de cuerpos porfídicos intrusivos en la formación Saldaña. *Boletín Geológico* **44**, 5–23.

Rodríguez-García G, Correa-Martínez AM, Zapata-Garcia G, Arango-Mejía MI, Obando-Erazo G, Zapata-Villada JP and Bermudez JG (2020a) Diverse Jurassic magmatic arcs of the Colombian Andes: constraints from petrography, geochronology, and geochemistry. In *The Geology of Colombia, Volume 2 Mesozoic* (eds J. Gómez and D. Mateus–Zabala), pp. 56–74. Servicio Geológico Colombiano, Publicaciones Geológicas Especiales 35.

Rodríguez-García G, Correa-Martinez AM, Zapata-Garcia G, Arango-Mejía MI, Obando-Erazo G, Zapata-Villada JP and Bermudez JG (2020b) Diverse Jurassic magmatic arcs of the colombian Andes constraints from petrography, geochronology, and geochemistry. In *The Geology of Colombia, Volume 2 Mesozoic* (eds J. Gómez and D. Mateus–Zabala), pp. 117–170. Servicio Geológico Colombiano, Publicaciones Geológicas Especiales 35.

Rodríguez-García G, Ramírez DA, Zapata JP, Correa-martínez AM, Sabrica C, Obando G, Estudios GD, Especiales G and Colombiano SG (2022) Redefinición, correlación e implicaciones geotectónicas del batolito de Ibagué, Colombia. Boletin de Geología 44, 65–93.

Rodríguez G, Zapata G, Arango MI and Bermúdez JG (2017) Caracterización petrográfica, geoquímica y geocronología de rocas granitoides pérmicas al occidente de la Plata y Pacaní - Huila, Valle Superior del Magdalena - Colombia. *Boletín de Geología* **39**, 41–68.

Rodríguez G, Arango MI, Zapata G and Bermúdez JG (2018) Petrotectonic characteristics, geochemistry, and U-Pb geochronology of Jurassic plutons in the Upper Magdalena Valley-Colombia: implications on the evolution of magmatic arcs in the NW Andes. *Journal of South American Earth Sciences* **81**, 10–30.

Saeid E, Bakioglu KB, Kellogg J, Leier A, Martinez JA and Guerrero E (2017) Garzón Massif basement tectonics: structural control on evolution of petroleum systems in upper Magdalena and Putumayo basins, Colombia. *Marine and Petroleum Geology* **88**, 381–401.

Schaaf P, Corona-Chávez P, Ortiz Joya G, Solís-Pichardo G, Arrieta García G, Hernández Treviño T and Poli S (2021) Magma hybridization, mingling, and recycling in the Manzanillo plutonic complex, Mexican Cordillera. *International Geology Review* **00**, 1–22.

Schmidt MW (1992) Amphibole composition in tonalite as a function of pressure: an experimental calibration of the Al-in-hornblende barometer. *Contributions to Mineralogy and Petrology* **110**, 304–310.

Sisson TW and Grove TL (1993) Experimental investigations of the role of H2O in calc-alkaline differentiation and subduction zone magmatism. *Contributions to Mineralogy and Petrology* **113**, 143–166.

Sousa CS, Conceição H, Soares HS, Fernandes DM and da Silva Rosa MD (2022) Magmatic processes recorded in plagioclase crystals of the Rio Jacaré Batholith, Sergipano Orogenic System, Northeast Brazil. *Journal of South American Earth Sciences* **118**, 103942.

Spikings R and Paul A (2019) The Permian – Triassic history of magmatic rocks of the Northern Andes (Colombia and Ecuador): supercontinent assembly and disassembly. In *The Geology of Colombia, Volume 2 Mesozoic* (eds D Gómez and J Mateus–Zabala), pp 1–43. Bogotá: Servicio Geológico Colombiano.

Spikings R, Cochrane R, Villagomez D, Van der Lelij R, Vallejo C, Winkler W and Beate B (2015) The geological history of northwestern South America: from Pangaea to the early collision of the Caribbean large igneous province (290-75 Ma). *Gondwana Research* **27**, 95–139.

Stolper E and Newman S (1994) The role of water in the petrogenesis of Mariana trough magmas. *Earth and Planetary Science Letters* **121**, 293–325.

Streckeisen A (1976) To each plutonic rock its proper name. *Earth-Science Reviews* **12**, 1–33. https://doi.org/10.1016/0012-8252(76)90052-0

Tischendorf G, Rieder M, Foster H, Gottesmann B and Guidotti VC (2004) A new graphical presentation and subdivision of potassium micas. *Mineralogical Magazine* **68**, 649–667.

Tischendorf G, Förster H-J, Gottesmann B and Rieder M (2007) True and brittle micas: composition and solid-solution series. *Mineralogical Magazine* **71**, 285–320.

Ulbrich H, Vlach SR and Janasi VDA (2001) O mapeamento faciológico em rochas ígneas plutônicas. *Revista Brasileira de Geociencias* **31**, 163–172.

Valencia-Gómez JC, Cardona A, Zapata S, Monsalve G, Marín D, Rodríguez-Cuevas M, Sobel ER, Parra M and Glodny J (2024) Fracture analysis and low-temperature thermochronology of faulted Jurassic igneous rocks in the Southern Colombian Andes: reservoir and tectonic implications. *Marine and Petroleum Geology* **165**, 106850.

Villamizar-Escalante N, Bernet M, Urueña-Suárez C, Hernández-González JS, Terraza-Melo R, Roncancio J, Muñoz JA, Peña ML, Amaya S and Piraquive A (2021) Thermal history of the southern Central Cordillera and its exhumation record in the Cenozoic deposits of the Upper Magdalena Valley, Colombia. *Journal of South American Earth Sciences* **107**, 103105.

Wang X, Hou T, Wang M, Zhang C, Zhang Z, Pan R, Marxer F and Zhang H (2021) A new clinopyroxene thermobarometer for mafic to intermediate magmatic systems. *European Journal of Mineralogy* **33**, 621–637.

Warr LN (2021) IMA–CNMNC approved mineral symbols. *Mineralogical Magazine* **85**, 291–320. https://doi.org/10.1180/mgm.2021.43

Waters LE and Lange RA (2016) No effect of H2O degassing on the oxidation state of magmatic liquids. *Earth and Planetary Science Letters* **447**, 48–59.

Wieser PE, Kent AJR and Till CB (2023) Barometers behaving badly II: a critical evaluation of Cpx-only and Cpx-Liq thermobarometry in variably-hydrous arc magmas. *Journal of Petrology* **64**, 1–25.

Wones DR (1989) Significance of the assemblage titanite + magnetite + quartz in granitic rocks. *American Mineralogist* **74**, 744–749.

Yan M, Wei J, Zhang D, Zhao Z, Turlin F, Li H, Li G, Xu C, Zhang X and Moritz R (2022) Petrogenesis of Late Devonian I- and A-type granitoids, and associated mafic microgranular enclaves in the northwestern North Qaidam Orogenic Belt, China: implications for continental crust growth during the post-collisional stage. *Lithos* **430**, 106857.

Zaheri–Abdehvand N, Hassanpour S, Rassa I and Rajabpour S (2022) Silicates chemistry as indicators of physicochemical and geothermometry conditions on porphyry ore system: a case study of the Haftcheshmeh Cu–Mo deposit, NW Iran. *Ore Geology Reviews* **142**, 104716.

Zandomeni PS, Moreno JA, Verdecchia SO, Baldo EG, Dahlquist JA, Morales Cámera MM, Balbis C, Benítez M, Serra-Varela S and Lembo Wuest CI (2021) Crystallization conditions and petrogenetic characterization of metaluminous to peraluminous calc-alkaline orogenic granitoids from mineralogical systematics: the case of the cambrian magmatism from the sierra de Guasayán (Argentina). *Minerals* **11**, 1–21.

Zapata-García G, Rodríguez-García G and Arango-Mejía MI (2017) Petrografía, geoquímica y geocronología de rocas metamórficas aflorantes en San Francisco Putumayo y la vía Palermo-San Luis asociadas a los complejos La Cocha – Río Téllez y Aleluya. *Boletín de Ciencias de la Tierra* **41**, 48–65.

Zapata S, Cardona A, Jaramillo C, Valencia V and Vervoort J (2016) U-Pb LA-ICP-MS geochronology and geochemistry of Jurassic volcanic and plutonic rocks from the Putumayo region (southern Colombia): tectonic setting and regional correlations. *Boletin de Geologia* **38**, 21–38.

Zapata S, Patiño A, Cardona A, Parra M, Valencia V, Reiners P, Oboh-Ikuenobe F and Genezini F (2020) Bedrock and detrital zircon thermochronology to unravel exhumation histories of accreted tectonic blocks: an example from the Western Colombian Andes. *Journal of South American Earth Sciences* **103**, 102715.

Zapata S, Zapata-Henao M, Cardona A, Jaramillo C, Silvestro D and Oboh-Ikuenobe F (2021) Long-term topographic growth and decay constrained by 3D thermo-kinematic modeling: tectonic evolution of the Antioquia Altiplano, Northern Andes. *Global and Planetary Change* **203**, 103553.

Zapata S, Calderon-Diaz L, Jaramillo C, Oboh-Ikuenobe F, Piedrahita JC, Rodríguez-Cuevas M, Cardona A, Sobel ER, Parra M, Valencia V, Patiño A, Jaramillo-Rios JS, Flores M and Glodny J (2023) Drainage and sedimentary response of the Northern Andes and the Pebas system to Miocene strike-slip tectonics: a source to sink study of the Magdalena Basin. *Basin Research* **35**, 1–44.

Zimmer MM, Plank T, Hauri EH, Yogodzinski GM, Stelling P, Larsen J, Singer B, Jicha B, Mandeville C and Nye CJ (2010) The role of water in generating the calc-alkaline trend: new volatile data for aleutian magmas and a new tholeiitic index. *Journal of Petrology* **51**, 2411–2444.